

# Renormalization-group improved predictions for Higgs boson production at large $p_T$

Fa Peng Huang,<sup>1</sup> Chong Sheng Li\*,<sup>1,2</sup> Hai Tao Li,<sup>1</sup> and Jian Wang<sup>3</sup>

<sup>1</sup>*School of Physics and State Key Laboratory of Nuclear Physics and Technology,  
Peking University, Beijing, 100871, China*

<sup>2</sup>*Center for High Energy Physics, Peking University, Beijing, 100871, China*

<sup>3</sup>*PRISMA Cluster of Excellence & Mainz Institut for Theoretical Physics,  
Johannes Gutenberg University, D-55099 Mainz, Germany*

We study the next-to-next-to-leading logarithmic order resummation for the large  $p_T$  Higgs boson production at the LHC in the framework of soft-collinear effective theory. We find that the resummation effects reduce the scale uncertainty significantly and decrease the QCD NLO results by about 11% in the large  $p_T$  region. The finite top quark mass effects and the effects of the NNLO singular terms are also discussed.

PACS numbers: 12.38.Cy, 14.80.Bn

---

\* Electronic address: csli@pku.edu.cn

## I. INTRODUCTION

In the standard model (SM), the Higgs boson is predicted by the Higgs mechanism in which the would-be Goldstones become the longitudinal components of the  $W$  and  $Z$  bosons. Although the existence of Higgs boson has been proposed for a long time, searching for this particle in the experiments has failed until the recent discovery at the LHC [1, 2]. In general, the Higgs boson may not be responsible for the mass origin of the fermions, and the current experimental data still allow the couplings of the Higgs boson with the fermions to deviate from the SM ones, especially, the coupling of the Higgs boson to the top quark [3]. Therefore, precise measurements of the couplings of the Higgs boson with other SM particles will test the Higgs mechanism in the SM [4–7].

The global fit method with current experiment data about the Higgs boson production and decay in various channels only provides indirect information on the top quark Yukawa coupling, which suffers from ambiguities from unknown new particles propagating in the loops. The most direct process to determine the coupling of the Higgs boson to the top quark is the  $t\bar{t}$  associated production  $pp \rightarrow t\bar{t}H$  and single top associated production  $pp \rightarrow tjH$ . However, the current abilities to measure the coupling of Higgs boson to the top quark through  $t\bar{t}$  associated production are still weak [3, 8] because of its small production cross section and complicated final states with copious decay products. The single top associated production has even smaller cross section because of the electro-weak interactions there, and is very challenging to measure.

Recently, a complementary method to determine the coupling of the Higgs boson to the top quark has been proposed in Refs. [5–7] by investigating the large  $p_T$  behavior of the Higgs boson in the process  $pp \rightarrow H + X$  with  $H \rightarrow ZZ^* \rightarrow l^+l^-l^+l^-$ . This method is feasible because the top quark mass can not be taken to be infinity when the Higgs boson has a large  $p_T$ . The top quark Yukawa coupling can be detected from the measurement of the variable [5]

$$r_{\pm} = \frac{N^+/N^-}{\sigma_{\text{SM}}^+/\sigma_{\text{SM}}^-}, \quad (1)$$

where  $N^{\pm}$  is the number of events in which the Higgs boson  $p_T$  is larger or smaller than a critical value  $P_T$ , for example,  $P_T = 300$  GeV.  $\sigma_{\text{SM}}^{\pm}$  is the corresponding theoretical predictions in the SM. It is pointed out that [5] the  $K$  factor, defined as the ratio of higher order results to the LO ones, for the Higgs boson  $p_T$  distribution is roughly  $p_T$  independent and very large, about 2, and that the resummation effects are negligible in the  $p_T$  range they considered. All these arguments are based on the calculation by the HqT program [9]. However, the resummation scheme used in the HqT program is only valid in the small  $p_T$  region, which is much less than 100 GeV. The

resummation prediction on the Higgs boson  $p_T$  distribution in the large  $p_T$  region, larger than 100 GeV, is investigated using the traditional method at next-to-leading-logarithm (NLL) [10]. The resummed logarithms are different in the small and large  $p_T$  regions. When the Higgs boson  $p_T$  is small, the threshold region is defined as  $z = M_H^2/s \rightarrow 1$ , where  $\sqrt{s}$  is the center-of-mass energy of the colliding partons. In the threshold region, only the soft gluon radiation is allowed, which leads to large logarithms  $\alpha_s^n \ln^{2n-m}(1-z)$ . In contrast, in the large  $p_T$  regions, the large logarithms are  $\alpha_s^n \ln^{2n-m}(1-y)$  with  $y = (p_T + m_T)^2/s$ , where  $m_T = \sqrt{p_T^2 + M_H^2}$  [10]. It is easy to observe that  $y \rightarrow 1$  does not necessarily lead to  $z \rightarrow 1$ , which means that the HqT program can not resum the large logarithms in the large  $p_T$  regions.

Notice that when the recoiling hardest jet against the Higgs boson is observed and additional jets are vetoed, there is a new kind of large Sudakov logarithms  $\alpha_s^n \ln^{2n-m} p_T/p_T^{\text{veto}}$ , which can be resummed [11–13]. If the mass of the jet is also measured, denoted as  $m_J$ , additional logarithms  $\ln^n m_J^2/p_J^2$  have been resummed up to next-to-next-to-leading-logarithm (NNLL) [14].

In this paper, we provide the resummed prediction for  $pp \rightarrow H + X$  at large  $p_T$  regions up to NNLL, without explicit observation of a jet, in contrast with the case in [14]. We will work in the soft-collinear effective theory (SCET) [15–19]. In the threshold limits of large  $p_T$  Higgs boson production, the final state radiations and beam remnants are highly suppressed which leads to final states consisting of a Higgs boson and an inclusive jet, as well as the remaining soft radiations, and therefore to the appearance of the large logarithms in the cross section. Then the resummation effects should be taken into account to obtain more precise predictions. The preliminarily theoretical NNLO analyses have been performed in Ref. [20]. The resummation formalism in SCET is different from that used in Ref. [10]. In the threshold region, the partonic cross section can be factorized to a hard function times a convolution between jet and soft functions. Each part has an explicit theoretical field definition which can be calculated perturbatively. In particular, each function contains only a single energy scale so that there is no potential large logarithms in each of them. The relative scale hierarchy between different functions is alleviated by running from one to the other via renormalization group equations. As a consequence, the large logarithms of the ratio of the different scales can be resummed to all orders.

In principle, the top quark mass should be kept to be finite in all the theoretical predictions in the large  $p_T$  regions [5, 7, 21, 22]. But because of the difficulty in calculating massive loops, this is achieved only for the LO result [23, 24] and the NLO total cross section expanded in  $M_H/m_t$  [25]. The differential cross section is calculated only in the large top quark limit up to NLO [21, 21, 26–28]. More recently, a big progress is made by computing the NNLO total cross section of the

sub-process  $gg \rightarrow H + j$  [29]. Therefore, an approximated differential cross section with finite top quark mass beyond the LO is usually used, which is obtained by multiplying the LO differential cross section with finite top quark mass with a differential  $K$  factor, as done in Ref. [30]. We will take into account the finite top quark mass effects in the resummation predictions following this method.

The precision prediction on Higgs boson production at large  $p_T$  regions can not only test the top quark Yukawa coupling discussed above, but also be a probe of the new physics. For example, in the SM the large transverse momentum spectrum of the Higgs boson produced in gluon fusion can be quite different from one of the minimal supersymmetric standard model [31, 32]. Light particles beyond the SM can be probed via the ratio of the partially integrated Higgs transverse momentum distribution to the inclusive rate [33].

This paper is organized as follows. In Sec. II, we analyze the kinematics of the Higgs boson and one jet associated production and give the definition of the threshold region. In Sec. III, we present the factorization and resummation formalism in momentum space using SCET. In Sec. IV, we present the hard function, jet function and soft functions at NLO. Then, we study the scale independence of the final result analytically. In Sec. V, we discuss the numerical results for this process at the LHC. We conclude in Sec. VI.

## II. ANALYSIS OF KINEMATICS

First of all, we introduce the relevant kinematical variables needed in our analysis. The dominant partonic processes for the Higgs boson and one jet production are  $gg \rightarrow gH$ ,  $gq \rightarrow gH$  and  $g\bar{q} \rightarrow \bar{q}H$ . The LO Feynman diagrams for the  $gg \rightarrow gH$  process are shown in Fig. 1.



FIG. 1: LO Feynman diagrams for the  $gg$  channel.

It is convenient to define two lightlike vectors along the beam directions,  $n_a$  and  $n_b$ , which are related by  $n_a = \bar{n}_b$ . Then, we introduce initial collinear fields along  $n_a$  and  $n_b$  to describe the collinear particles in the beam directions. In the center-of-mass (c.m.) frame of the hadronic collision, the momenta of the incoming hadrons are given by

$$P_a^\mu = E_{\text{c.m.}} \frac{n_a^\mu}{2}, \quad P_b^\mu = E_{\text{c.m.}} \frac{n_b^\mu}{2}. \quad (2)$$

Here  $E_{\text{c.m.}}$  is the c.m. energy of the collider and we have neglected the masses of the hadrons. The momenta of the incoming partons, with a light-cone momentum fraction of the hadronic momentum, are

$$\tilde{p}_a = x_a E_{\text{c.m.}} \frac{n_a^\mu}{2}, \quad \tilde{p}_b = x_b E_{\text{c.m.}} \frac{n_b^\mu}{2}. \quad (3)$$

At the hadronic and partonic level, the momentum conservation gives

$$P_a + P_b = q + P_X, \quad (4)$$

and

$$\tilde{p}_a + \tilde{p}_b = q + p_X, \quad (5)$$

respectively, where  $q$  is the momentum of the Higgs boson. We define the partonic jet with jet momentum  $p_X$  to be the set of all final state partons except the Higgs boson in the partonic processes, while the hadronic jet with jet momentum  $P_X$  contains all the hadrons as well as the beam remnants in the final state except the Higgs boson.

We also define the Mandelstam variables as

$$s = (P_a + P_b)^2, \quad u = (P_a - q)^2, \quad t = (P_b - q)^2 \quad (6)$$

for hadrons, and

$$\hat{s} = (\tilde{p}_a + \tilde{p}_b)^2, \quad \hat{u} = (\tilde{p}_a - q)^2, \quad \hat{t} = (\tilde{p}_b - q)^2 \quad (7)$$

for partons, respectively. In terms of the Mandelstam variables, the hadronic and partonic threshold variables are defined as

$$S_4 \equiv P_X^2 = s + t + u - M_H^2, \quad (8)$$

$$s_4 \equiv p_X^2 = \hat{s} + \hat{t} + \hat{u} - M_H^2, \quad (9)$$

where  $M_H$  is the mass of the Higgs boson. The hadronic threshold limit is defined as  $S_4 \rightarrow 0$  [34]. In this limit, the final state radiations and beam remnants are highly suppressed, which leads to final states consisting of a Higgs boson and an energetic jet, as well as the remaining soft radiations. Taking this limit requires  $x_a \rightarrow 1$ ,  $x_b \rightarrow 1$ ,  $s_4 \rightarrow 0$  simultaneously, and we get

$$\begin{aligned} S_4 &= s_4 + \hat{s} \left( \frac{1}{x_a x_b} - 1 \right) + (\hat{t} - M_H^2) \left( \frac{1}{x_b} - 1 \right) + (\hat{u} - M_H^2) \left( \frac{1}{x_a} - 1 \right) \\ &\approx s_4 + \hat{s}(\bar{x}_a + \bar{x}_b) + (\hat{t} - M_H^2)\bar{x}_b + (\hat{u} - M_H^2)\bar{x}_a \\ &\approx s_4 + (-\hat{t})\bar{x}_a + (-\hat{u})\bar{x}_b, \end{aligned} \quad (10)$$

where  $\bar{x}_{a,b} = 1 - x_{a,b}$ . This expression can help to check the factorization scale invariance, which is shown in detail below. Near the partonic threshold, the boson must be recoiling against a jet and there is only phase space for the jet to be nearly massless. In this case,  $p_X = p_1 + k$ , where  $p_1$  is the momentum of the final state collinear partons forming the jet and  $k$  is the momentum of the soft radiations.

We note that in both hadronic and partonic threshold limit, the Higgs boson is not forced to be produced at rest, *i.e.* it can have a large momentum. Actually, as the momentum of the Higgs boson becomes larger and larger, the final-state phase space lies more close to the threshold limit. We point that the definition of the partonic threshold limit  $s_4/\hat{s} \rightarrow 0$  is different from the case of  $y \rightarrow 1$  [10], as discussed in the introduction. They are equivalent to each other only if the momentum component  $p_z$  of the Higgs boson in the partonic c.m. frame vanishes.

For convenience, we can also write the threshold variable as

$$s_4 = p_X^2 = (\tilde{p}_a + \tilde{p}_b - q)^2 = p_1^2 + 2k^+ E_1 + \mathcal{O}(k^2), \quad (11)$$

where  $k^+ = n_1 \cdot k$ ,  $k$  is the momentum of soft radiations,  $E_1$  is the energy of the jet and  $n_1$  is the lightlike vector associated with the jet direction. In the threshold limit ( $s_4 \rightarrow 0$ ), incomplete cancelation of the divergences between real and virtual corrections leads to singular distributions  $\alpha_s^n [\ln^m(s_4/M_H^2)/s_4]_+$ , with  $m \leq 2n - 1$ . It is the purpose of threshold resummation to sum up these contributions to all orders in  $\alpha_s$ .

The total cross section is given by

$$\begin{aligned} \sigma &= \int dx_a \int dx_b \int d\hat{t} \int d\hat{u} f_{i/P_a}(\mu_F, x_a) f_{j/P_b}(\mu_F, x_b) \frac{1}{2\hat{s}} \frac{d\hat{\sigma}_{ij}}{d\hat{t}d\hat{u}} \\ &= \int_0^{p_{T,\max}^2} dp_T^2 \int_{-y_{\max}}^{y_{\max}} dy \int_{x_{b,\min}}^1 dx_b \int_0^{s_4^{\max}} ds_4 \frac{1}{2(x_b s + u - M_H^2)} f_{i/P_a}(\mu_F, x_a) f_{j/P_b}(\mu_F, x_b) \frac{d\hat{\sigma}_{ij}}{d\hat{t}d\hat{u}}, \end{aligned} \quad (12)$$

where we have changed the integration variables into the Higgs boson transverse momentum squared  $p_T^2$ , rapidity  $y$ ,  $x_b$  and  $s_4$ . The regions of the integration variables are given by

$$\begin{aligned} p_{T,\max}^2 &= \frac{(s - M_H^2)^2}{4s}, \\ y_{\max} &= \frac{1}{2} \ln \frac{1 + \sqrt{1 - \xi}}{1 - \sqrt{1 - \xi}}, \\ x_{b,\min} &= \frac{-u}{s + t - M_H^2}, \\ s_4^{\max} &= x_b(s + t - M_H^2) + u, \end{aligned} \quad (13)$$

with

$$\begin{aligned}\xi &= \frac{4s(p_T^2 + M_H^2)}{(s + M_H^2)^2}, \\ t &= M_H^2 - \sqrt{s}\sqrt{p_T^2 + M_H^2}e^y, \\ u &= M_H^2 - \sqrt{s}\sqrt{p_T^2 + M_H^2}e^{-y}.\end{aligned}\tag{14}$$

The other kinematical variables can be expressed in terms of these four integration variables.

### III. FACTORIZATION AND RESUMMATION FORMALISM IN SCET

In the frame of SCET, we define a small expanded parameter  $\lambda = \sqrt{s_4}/Q$  ( $\lambda \ll 1$ ) in the threshold limit  $s_4 \rightarrow 0$ . Here,  $Q$  is the characteristic energy of the hard scattering process. The momentum of a collinear particle scales as

$$\text{collinear : } p_c^\mu \sim Q(1, \lambda^2, \lambda),\tag{15}$$

and the momentum of a soft particle scales as

$$\text{soft : } p_s^\mu \sim Q(\lambda^2, \lambda^2, \lambda^2).\tag{16}$$

The soft fields scale as  $\psi_s \sim \lambda^3$ ,  $A_s \sim \lambda^2$ , and the collinear fermion field  $\psi_c$  scales as  $\lambda$ . The light-cone components of the collinear gluon field  $A_c^\mu$  scale the same way as its momentum  $p_c^\mu$  in covariant gauge.

The soft gluon field are multipole expanded around  $x_-$  to maintain a consistent power counting in  $\lambda$ . Thus, the soft gluon operator depends only on  $x_-^\mu = (\bar{n}_J \cdot x) \frac{n_J^\mu}{2}$  at leading power, and its Fourier transform only depends on  $k_+ = n_J \cdot k$ . It is needed to mention that  $p_s^2 \sim Q^2 \lambda^2$  is of order of the jet mass and is assumed to be in the perturbative region.

In the limit of the infinite top quark mass, the effective Lagrangian of Higgs boson production via gluon fusion can be written as [26]

$$L = C_t(m_t, \mu) \frac{\alpha_s(\mu)}{12\pi} \frac{H}{v} \text{Tr}(G_{\mu\nu} G^{\mu\nu}),\tag{17}$$

with

$$C_t = 1 + \frac{11\alpha_s(\mu)}{4\pi},\tag{18}$$

where  $C_t$  is the Wilson coefficient at  $\alpha_s$  order. The leading power effective operator of  $gg \rightarrow gH$  in SCET is as follows,

$$\mathcal{O}_{abc}^{\alpha\beta\gamma}(x; t_1, t_2, t_J) = \mathcal{A}_{a\perp}^{\alpha 1}(x + t_1 \bar{n}_1) \mathcal{A}_{b\perp}^{\beta 2}(x + t_2 \bar{n}_2) \mathcal{A}_{c\perp}^{\gamma J}(x + t_J \bar{n}_J),\tag{19}$$

where  $\mathcal{A}_{a\perp}^{\alpha,i}$  is the effective gluon field in the frame of SCET. The corresponding hadronic operator can be written as

$$\mathcal{J}(x) = \int dt_1 dt_2 dt_J C_{\alpha\beta\gamma}^{abc}(t_1, t_2, t_J) \mathcal{O}_{abc}^{\alpha\beta\gamma}(x; t_1, t_2, t_J). \quad (20)$$

The generic expression of the cross section is

$$d\sigma = \frac{1}{2s} \left( \frac{\alpha_s C_t}{12\pi v} \right)^2 \frac{d^3 q}{(2\pi)^3 2E_H} \sum_X (2\pi)^4 \delta^{(4)}(P_1 + P_2 - p_X - q) \left| \langle X | \mathcal{J}(0) | N_1(P_1) N_2(P_2) \rangle \right|^2. \quad (21)$$

Substituting Eqs. (19)–(20) into Eq. (21) and performing Fourier transformation, we get

$$d\sigma = \frac{1}{2s} \left( \frac{\alpha_s C_t}{12\pi v} \right)^2 \frac{d^3 q}{(2\pi)^3 2E_H} \sum_X \tilde{C}_{\alpha\beta\gamma}^{abc*} \tilde{C}_{\mu\nu\rho}^{def} \times \int d^4 x e^{-i(qx)} \langle N_1(P_1) N_2(P_2) | \mathcal{O}_{\alpha\beta\gamma}^{abc\dagger}(x) | X \rangle \langle X | \mathcal{O}_{\mu\nu\rho}^{def}(0) | N_1(P_1) N_2(P_2) \rangle. \quad (22)$$

After redefining the field to decouple the soft interactions, the operator factorizes into a collinear and a soft part

$$\mathcal{O}_{abc}^{\alpha\beta\gamma} = \mathcal{O}^S \mathcal{O}_{abc}^{\alpha\beta\gamma C}, \quad (23)$$

where the collinear part  $\mathcal{O}_{abc}^{\alpha\beta\gamma C}$  has the same form as  $\mathcal{O}_{abc}^{\alpha\beta\gamma}$  in Eq. (19) with the collinear fields replaced by those not interacting with soft gluons, and the soft part  $\mathcal{O}^S = Y_1 Y_2 Y_J$ .  $Y_i$  is the soft Wilson lines defined as

$$Y_i(x) = \mathbf{P} \exp \left( ig \int_{-\infty}^0 dt n_i \cdot A_s^a(x + tn_i) \mathbf{T}_i^a \right), \quad (24)$$

where  $\mathbf{P}$  indicates path ordering. From here, we omit the color index for simplicity, and we rewrite the squared amplitude in Eq. (22) as

$$\begin{aligned} \langle N_1(P_1) N_2(P_2) | \mathcal{O}_{\alpha\beta\gamma}^\dagger(x) | X \rangle \langle X | \mathcal{O}_{\mu\nu\rho}(0) | N_1(P_1) N_2(P_2) \rangle = \\ \left\langle N_1(P_1) \left| \mathcal{A}_{1\alpha}^\perp(x) \mathcal{A}_{1\mu}^\perp(0) \right| N_1(P_1) \right\rangle \times \left\langle N_2(P_2) \left| \mathcal{A}_{2\beta}^\perp(x) \mathcal{A}_{2\nu}^\perp(0) \right| N_2(P_2) \right\rangle \\ \times \sum_{X_c} \langle 0 | \mathcal{A}_{J\gamma}^\perp(x) | X_c \rangle \langle X_c | \mathcal{A}_{J\rho}^\perp(0) | 0 \rangle \times \sum_{X_s} \langle 0 | \mathcal{O}_{gg}^{s\dagger}(x) | X_s \rangle \langle X_s | \mathcal{O}_{gg}^s(0) | 0 \rangle. \end{aligned} \quad (25)$$

Substituting the definition of the gluon jet function, soft function, parton distribution functions (PDFs) and hard function into Eq. (25),

$$\sum_{X_c} \langle 0 | \mathcal{A}_{J\gamma}^\perp(x) | X_c \rangle \langle X_c | \mathcal{A}_{J\rho}^\perp(0) | 0 \rangle \propto (-g_{\gamma\rho}^\perp) \int \frac{d^4 p}{(2\pi)^3} \theta(p^0) J_g(p^2) e^{-i x p}, \quad (26)$$

$$\sum_{X_s} \langle 0 | \mathcal{O}_{gg}^{s\dagger}(x) | X_s \rangle \langle X_s | \mathcal{O}_{gg}^s(0) | 0 \rangle \propto \int_0^\infty dk_+ e^{-ik_+(\bar{n}_J \cdot x)/2} \mathcal{S}_{gg}(k_+), \quad (27)$$



$$\langle N_i(P_i) | (-g_{\mu\nu}) \mathcal{A}_{i\perp}^\mu \left( n_i \cdot x \frac{\bar{n}_i^\mu}{2} \right) \mathcal{A}_{i\perp}^\nu(0) | N_i(P_i) \rangle = \int_{-1}^1 \frac{d\xi}{\xi} f_{g/N_i}(\xi) e^{i\xi(n_i \cdot x)(\bar{n}_i \cdot P_i)/2}, \quad (28)$$

we obtain (up to power corrections) [35, 36]

$$\sigma = \int dx_a dx_b d\hat{t} d\hat{u} \frac{1}{2\hat{s}} f_{i/P_a}(x_a, \mu) f_{j/P_b}(x_b, \mu) \frac{d\hat{\sigma}_{ij}^{\text{thres}}}{d\hat{t} d\hat{u}}, \quad (29)$$

$$\begin{aligned} \frac{d\hat{\sigma}_{ij}^{\text{thres}}}{d\hat{t} d\hat{u}} &= \frac{1}{8\pi} \frac{1}{\hat{s}} \lambda_{0,ij} H_{ij}(\mu) \\ &\times \int dk^+ \int dp_1^2 \mathcal{S}(k^+, \mu) J(p_1^2, \mu) \delta(s_4 - p_1^2 - 2k^+ E_1), \end{aligned} \quad (30)$$

with

$$\lambda_{0,gg} = \frac{1}{2^2(N_c^2 - 1)^2} \frac{\alpha_s^3}{9\pi v^2} \frac{4N_c(N_c^2 - 1)(M_H^8 + \hat{s}^4 + \hat{t}^4 + \hat{u}^4)}{\hat{s}\hat{t}\hat{u}}, \quad (31)$$

$$\lambda_{0,gq} = \frac{1}{2^2 N_c(N_c^2 - 1)} \frac{\alpha_s^3}{9\pi v^2} \frac{2(N_c^2 - 1)(\hat{s}^2 + \hat{u}^2)}{-\hat{t}}, \quad (32)$$

where  $\lambda_{0,ij}$  is the squared amplitude at LO after averaging the spins and colors.

The other channels follow the same approach to obtain the factorization formulas. By crossing symmetry, the LO cross sections in other channels are obtained by

$$\lambda_{0,g\bar{q}} = \lambda_{0,gq}(\hat{s} \leftrightarrow \hat{u}), \quad (33)$$

$$\lambda_{0,q\bar{q}} = -\lambda_{0,gq}(\hat{s} \leftrightarrow \hat{t}). \quad (34)$$

Here, we point out that the factorization form given in Eq.(30) is only valid in the threshold limit defined by  $s_4 \rightarrow 0$ , which means that the Higgs boson should have a large  $p_T$ . The traditional transverse momentum dependent factorization and resummation [37, 38] is important when the total transverse momentum of the Higgs boson and the recoiling jet is small, that is obvious not the same threshold region as the case we have discussed in this paper. An application of the transverse momentum resummation in Higgs plus one jet production has been discussed in [11–13, 39].

#### IV. THE HARD, JET AND SOFT FUNCTIONS AT NLO

The hard, jet and soft functions describe interactions at different scales, which can be calculated order by order in QCD, respectively. At the NNLL accuracy, we need the explicit expressions of the hard, jet and soft functions up to NLO. In this section, we summarize the relevant analytic results of them.



FIG. 2: The sample one-loop Feynman diagrams for the subprocess  $gg \rightarrow gH$ .

### A. Hard functions

The hard functions are absolute value squared of the Wilson coefficients of the operators, which can be obtained by matching the full theory onto SCET. It is obtained by subtracting the IR divergences in the  $\overline{MS}$  scheme from the UV renormalized amplitudes of the full theory. At the LO, the hard function  $H$  is normalized to 1. In general, it is related to the amplitudes of the full theory, using

$$\begin{aligned}\lambda_{0,ij}H_{IJ}^{(0)} &= \frac{1}{\langle c_I|c_I\rangle\langle c_J|c_J\rangle}\langle c_I|\mathcal{M}_{\text{ren}}^{(0)}\rangle\langle\mathcal{M}_{\text{ren}}^{(0)}|c_J\rangle, \\ \lambda_{0,ij}H_{IJ}^{(1)} &= \frac{1}{\langle c_I|c_I\rangle\langle c_J|c_J\rangle}\left(\langle c_I|\mathcal{M}_{\text{ren}}^{(1)}\rangle\langle\mathcal{M}_{\text{ren}}^{(0)}|c_J\rangle + \langle c_I|\mathcal{M}_{\text{ren}}^{(0)}\rangle\langle\mathcal{M}_{\text{ren}}^{(1)}|c_J\rangle\right),\end{aligned}\quad (35)$$

where  $|\mathcal{M}_{\text{ren}}\rangle$  are obtained by subtracting the IR divergences in the  $\overline{MS}$  scheme from the UV renormalized amplitudes of the full theory [40–42]. At NLO, in practice, it is necessary to calculate the one-loop on-shell Feynman diagrams of this process, as shown in Fig. 2. Using the one-loop results in Refs. [21, 26], we get the hard functions at NLO as follows

$$\begin{aligned}H_{gg}(\mu_h) &= 1 + \frac{\alpha_s(\mu_h)}{4\pi}\left\{-3N_c\ln^2\left(\frac{\mu_h^2}{M_H^2}\right)\right. \\ &\quad \left.+ \left[\gamma_{gg}^{H,0} - 2N_c\left(\ln\left(\frac{M_H^2}{\hat{s}}\right) + \ln\left(\frac{M_H^2}{-\hat{t}}\right) + \ln\left(\frac{M_H^2}{-\hat{u}}\right)\right)\right]\ln\left(\frac{\mu_h^2}{M_H^2}\right) + c_1^{H,gg}\right\},\end{aligned}\quad (36)$$

$$\begin{aligned}H_{gq}(\mu_h) &= 1 + \frac{\alpha_s(\mu_h)}{4\pi}\left[\left(\frac{1}{N_c} - 2N_c\right)\ln^2\left(\frac{\mu_h^2}{M_H^2}\right)\right. \\ &\quad \left.+ \frac{N_c^2\left(-6\ln\left(\frac{M_H^2}{\hat{s}}\right) - 6\ln\left(\frac{M_H^2}{-\hat{u}}\right) + 13\right) + 6\ln\left(\frac{M_H^2}{-\hat{t}}\right) - 4N_cn_f + 9}{3N_c}\ln\left(\frac{\mu_h^2}{M_H^2}\right) + c_1^{H,gq}\right],\end{aligned}\quad (37)$$

with

$$\begin{aligned}
c_1^{H,gg} = & 3 \left[ 4\text{Li}_2 \left( 1 - \frac{M_H^2}{\hat{s}} \right) + 4\text{Li}_2 \left( \frac{\hat{u}}{M_H^2} \right) + 4\text{Li}_2 \left( \frac{\hat{t}}{M_H^2} \right) + \ln^2 \left( \frac{M_H^2}{\hat{s}} \right) - \ln^2 \left( \frac{M_H^2}{-\hat{u}} \right) \right. \\
& - \ln^2 \left( \frac{M_H^2}{-\hat{t}} \right) - 2 \ln \left( \frac{\hat{s}}{M_H^2} \right) \ln \left( \frac{-\hat{u}}{M_H^2} \right) - 2 \ln \left( \frac{\hat{s}}{M_H^2} \right) \ln \left( \frac{-\hat{t}}{M_H^2} \right) - 2 \ln \left( \frac{-\hat{u}}{M_H^2} \right) \ln \left( \frac{-\hat{t}}{M_H^2} \right) \\
& + 4 \ln \left( \frac{-\hat{u}}{M_H^2} \right) \ln \left( 1 - \frac{\hat{u}}{M_H^2} \right) + 4 \ln \left( \frac{-\hat{t}}{M_H^2} \right) \ln \left( 1 - \frac{\hat{t}}{M_H^2} \right) + \frac{25\pi^2}{6} \Big] \\
& + \frac{2(N_c - n_f)M_H^2[M_H^2(\hat{s}\hat{t} + \hat{s}\hat{u} + \hat{t}\hat{u}) + \hat{s}\hat{t}\hat{u}]}{3(M_H^8 + \hat{s}^4 + \hat{t}^4 + \hat{u}^4)} + 22
\end{aligned} \tag{38}$$

$$c_1^{H,gq} = N_c V_1 + \frac{1}{N_c} V_2 + n_f V_3 + V_4, \tag{39}$$

where

$$\begin{aligned}
V_1 = & 4\text{Li}_2 \left( 1 - \frac{\hat{t}}{M_H^2} \right) + 2\text{Li}_2 \left( 1 - \frac{\hat{u}}{M_H^2} \right) + 2\text{Li}_2 \left( 1 - \frac{\hat{s}}{M_H^2} \right) - \frac{13}{3} \ln \left( \frac{-\hat{t}}{M_H^2} \right) \\
& - \ln^2 \left( \frac{M_H^2}{-\hat{u}} \right) - 2 \ln \left( \frac{-\hat{t}}{M_H^2} \right) \ln \left( \frac{-\hat{u}}{M_H^2} \right) - 2 \ln \left( \frac{\hat{s}}{M_H^2} \right) \ln \left( \frac{-\hat{t}}{M_H^2} \right) \\
& + 4 \ln \left( 1 - \frac{\hat{t}}{M_H^2} \right) \ln \left( \frac{-\hat{t}}{M_H^2} \right) + 2 \ln \left( 1 - \frac{\hat{u}}{M_H^2} \right) \ln \left( \frac{-\hat{u}}{M_H^2} \right) + \frac{80}{9},
\end{aligned} \tag{40}$$

$$\begin{aligned}
V_2 = & -2\text{Li}_2 \left( 1 - \frac{\hat{s}}{M_H^2} \right) - 2\text{Li}_2 \left( 1 - \frac{\hat{u}}{M_H^2} \right) + \ln^2 \left( \frac{M_H^2}{-\hat{t}} \right) - \ln^2 \left( \frac{M_H^2}{\hat{s}} \right) - 3 \ln \left( \frac{-\hat{t}}{M_H^2} \right) \\
& + 2 \ln \left( \frac{\hat{s}}{M_H^2} \right) \ln \left( \frac{-\hat{u}}{M_H^2} \right) - 2 \ln \left( 1 - \frac{\hat{u}}{M_H^2} \right) \ln \left( \frac{-\hat{u}}{M_H^2} \right) - \frac{\pi^2}{6} + 8,
\end{aligned} \tag{41}$$

$$V_3 = \frac{4}{3} \ln \left( \frac{-\hat{t}}{M_H^2} \right) - \frac{20}{9}, \tag{42}$$

$$V_4 = \frac{10 - \hat{t}(\hat{u} + \hat{s})}{3 \hat{u}^2 + \hat{s}^2} + 22. \tag{43}$$

Our results of hard functions are consistent with the results in Ref [14]. The hard functions at the other scales can be obtained by evolution of renormalization group (RG) equations. The RG equations for hard functions are governed by the anomalous-dimension matrix, which has been calculated in Refs. [43–48]. In our case, the RG equations for hard functions are given by

$$\frac{d}{d \ln \mu_h} H_{gg}(\mu_h) = \left[ 3\gamma_{\text{cusp}} \left( \ln \frac{\hat{s}}{\mu_h^2} + \ln \frac{-\hat{t}}{\mu_h^2} + \ln \frac{-\hat{u}}{\mu_h^2} \right) + 2\gamma_{gg}^H \right] H_{gg}(\mu_h), \tag{44}$$

$$\frac{d}{d \ln \mu_h} H_{gq}(\mu_h) = \left[ 3\gamma_{\text{cusp}} \left( \ln \frac{\hat{s}}{\mu_h^2} + \ln \frac{-\hat{u}}{\mu_h^2} - \frac{1}{9} \ln \frac{-\hat{t}}{\mu_h^2} \right) + 2\gamma_{gq}^H \right] H_{gq}(\mu_h), \tag{45}$$

with

$$2\gamma_{gg}^H = 2\gamma_{gg}^V - 3 \frac{\beta(\alpha_s)}{\alpha_s}, \quad \gamma_{gg}^{H,0} = 0, \tag{46}$$

$$2\gamma_{gq}^H = 2\gamma_{gq}^V - 3 \frac{\beta(\alpha_s)}{\alpha_s}, \quad \gamma_{gq}^{H,0} = -6C_F + 2\beta_0, \tag{47}$$

where  $\gamma_{\text{cusp}}$  is the universal anomalous-dimension function related to the cusp anomalous dimension of Wilson loops with lightlike segments [49–51], while  $\gamma_{gg}^V$  and  $\gamma_{gq}^V$  control the single-logarithmic evolution. Their explicit expressions are shown in Ref. [47]. In the following, all anomalous dimensions are expanded in unit of  $\alpha_s/4\pi$ , for example,  $\gamma_{\text{cusp}}(\alpha) = \frac{\alpha_s}{4\pi}\Gamma_0 + (\frac{\alpha_s}{4\pi})^2\Gamma_1 + \mathcal{O}(\alpha_s^3)$ .

Solving the RG equations, the hard function at an arbitrary scale  $\mu$  are given by:

$$H_{gg}(\mu) = \left(\frac{\alpha_s(\mu_h)}{\alpha_s(\mu)}\right)^3 \exp[18S(\mu_h, \mu) - 2a_{gg}^V(\mu_h, \mu)] \left(\frac{\hat{s}\hat{t}\hat{u}}{\mu_h^6}\right)^{-3a_\Gamma(\mu_h, \mu)} H_{gg}(\mu_h), \quad (48)$$

$$H_{gq}(\mu) = \left(\frac{\alpha_s(\mu_h)}{\alpha_s(\mu)}\right)^3 \exp\left[\frac{34}{3}S(\mu_h, \mu) - 2a_{gq}^V(\mu_h, \mu)\right] \left(\frac{(\hat{s})^9(-\hat{u})^9/(-\hat{t})}{\mu_h^{34}}\right)^{-\frac{1}{3}a_\Gamma(\mu_h, \mu)} H_{gq}(\mu_h), \quad (49)$$

where  $S(\mu_h, \mu)$  and  $a_{gi}^V$  are defined as [52]

$$S(\mu_h, \mu) = - \int_{\alpha_s(\mu_h)}^{\alpha_s(\mu)} d\alpha \frac{\gamma_{\text{cusp}}(\alpha)}{\beta(\alpha)} \int_{\alpha_s(\mu_h)}^{\alpha} \frac{d\alpha'}{\beta(\alpha')}, \quad (50)$$

$$a_{gi}^V(\mu_h, \mu) = - \int_{\alpha_s(\mu_h)}^{\alpha_s(\mu)} d\alpha \frac{\gamma_{gi}^V(\alpha)}{\beta(\alpha)}. \quad (51)$$

The general hard function up to  $\mathcal{O}(\alpha_s^2)$  can be written as

$$\begin{aligned} \tilde{H}_{ij} = & 1 + \left(\frac{\alpha_s}{4\pi}\right) \left\{ -\rho_{ij}\Gamma_0 \frac{L_H^2}{2} - \tilde{\gamma}_0^{H_{ij}} L_H + c_1^H \right\} \\ & + \left(\frac{\alpha_s}{4\pi}\right)^2 \left\{ (\rho_{ij}\Gamma_0)^2 \frac{L_H^4}{8} + (\beta_0 + 3\tilde{\gamma}_0^{H_{ij}}) \rho_{ij}\Gamma_0 \frac{L_H^3}{6} \right. \\ & + \left[ \tilde{\gamma}_0^{H_{ij}}(\beta_0 + \tilde{\gamma}_0^{H_{ij}}) - \rho_{ij}\Gamma_1 - \rho_{ij}\Gamma_0 c_1^H \right] \frac{L_H^2}{2} \\ & \left. + \left[ -c_1^H(\beta_0 + \tilde{\gamma}_0^{H_{ij}}) - \tilde{\gamma}_1^{H_{ij}} \right] L_H + c_2^H \right\}. \end{aligned} \quad (52)$$

The coefficients in the above equation can be obtained from Refs.[20, 53]. Here,  $L_H = \ln\left(\frac{\mu_h^2}{M_H^2}\right)$ ,  $\rho_{gg} = 9/2$ ,  $\rho_{gq} = 17/6$ ,  $\tilde{\gamma}^{H_{gg}}(\alpha_s) = 3\gamma^g(\alpha_s) + \frac{C_A}{2}\Gamma \ln \frac{\hat{s}\hat{t}\hat{u}}{\mu_h^6} - \frac{3\beta(\alpha_s)}{2\alpha_s}$ ,  $\tilde{\gamma}^{H_{gq}}(\alpha_s) = 2\gamma^g(\alpha_s) + \gamma^q + \frac{C_A}{18}\Gamma \ln \frac{\hat{s}^9(-\hat{u})^9}{-t\mu_h^{34}} - \frac{3\beta(\alpha_s)}{2\alpha_s}$ .

## B. Jet function

The jet function of gluon  $J_g(p^2)$  is defined as

$$\langle 0 | \mathcal{A}_{J\perp}^{a\mu}(x) \mathcal{A}_{J\perp}^{b\nu}(0) | 0 \rangle = (-g_{\perp}^{\mu\nu}) \delta^{ab} g_s^2 \int \frac{d^4 p}{(2\pi)^3} \theta(p^0) J_g(p^2) e^{-ipx}. \quad (53)$$

These collinear gluon operators have nonvanishing matrix elements only for intermediate collinear states. Thus, this jet function can be considered as the result of integrating out the collinear

modes at the scale  $\mu_j$ . Equivalently, we can extract the jet function from the imaginary part of the time-ordered product of collinear fields

$$\frac{1}{\pi} \text{Im} \left[ i \int d^4x e^{ipx} \langle 0 | T \left\{ \mathcal{A}_{J\perp}^{a\mu}(x) \mathcal{A}_{J\perp}^{b\nu}(0) \right\} | 0 \rangle \right] = (-g_{\perp}^{\mu\nu}) \delta^{ab} g_s^2 J_g(p^2). \quad (54)$$

The RG evolution of the jet function is given by

$$\frac{dJ_i(p^2, \mu)}{d \ln \mu} = \left( -2\gamma_{\text{cusp}} \ln \frac{p^2}{\mu^2} - 2\gamma_i^J \right) J_i(p^2, \mu) + 2\gamma_{\text{cusp}} \int_0^{p^2} dq^2 \frac{J_i(p^2, \mu) - J_i(q^2, \mu)}{p^2 - q^2} \quad (55)$$

with  $i = g, q$ . To solve this integro-differential evolution equation, we use the Laplace transformed jet function [52]

$$\tilde{j}_i(\ln \frac{Q^2}{\mu^2}, \mu) = \int_0^\infty dp^2 \exp(-\frac{p^2}{Q^2 e^{\gamma_E}}) J_i(p^2, \mu), \quad (56)$$

which satisfies the the RG equation

$$\frac{d}{d \ln \mu} \tilde{j}_i(\ln \frac{Q^2}{\mu^2}, \mu) = \left( -2C_i \gamma_{\text{cusp}} \ln \frac{Q^2}{\mu^2} - 2\gamma_i^J \right) \tilde{j}_i(\ln \frac{Q^2}{\mu^2}, \mu). \quad (57)$$

The Laplace transformed jet function  $\tilde{j}_i(L, \mu)$  at NNLO [54, 55] is

$$\begin{aligned} \tilde{j}_i(L, \mu) = & 1 + \frac{\alpha_s}{4\pi} \left( \frac{C_i \Gamma_0}{2} L^2 + \gamma_0^{J_i} L + c_1^{J_i} \right) \\ & + \left( \frac{\alpha_s}{4\pi} \right)^2 \left\{ \frac{C_i^2 \Gamma_0^2}{8} L^4 + \left( \frac{\gamma_0^{J_i} C_i \Gamma_0}{2} - \frac{\beta_0 C_i \Gamma_0}{6} \right) L^3 + \frac{1}{2} [C_i \Gamma_1 + (\gamma_0^{J_i} - \beta_0) \gamma_0^{J_i} + c_1^{J_i} C_i \Gamma_0] L^2 \right. \\ & \left. + [\gamma_1^{J_i} + (\gamma_0^{J_i} - \beta_0) c_1^{J_i}] L + c_2^{J_i} \right\} \end{aligned} \quad (58)$$

with

$$\begin{aligned} c_1^{J_q} &= \left( 7 - \frac{2}{3} \pi^2 \right) C_F, \\ c_1^{J_g} &= \left( \frac{67}{9} - \frac{2}{3} \pi^2 \right) C_A - \frac{20}{9} n_f T_F, \\ c_2^{J_q} &= \left( \frac{205}{8} - \frac{97\pi^2}{12} + \frac{61\pi^4}{90} - 6\zeta_3 \right) C_F^2 + \left( \frac{53129}{648} - \frac{155\pi^2}{36} - \frac{37\pi^4}{180} - 18\zeta_3 \right) C_F C_A \\ &+ \left( -\frac{4057}{162} + \frac{13\pi^2}{9} \right) C_F n_f T_F, \end{aligned} \quad (59)$$

$$\begin{aligned} c_2^{J_g} &= C_A^2 \left( \frac{20215}{162} - \frac{362\pi^2}{27} - \frac{88\zeta_3}{3} + \frac{17\pi^4}{36} \right) + C_A n_f T_F \left( -\frac{1520}{27} + \frac{134\pi^2}{27} - \frac{16\zeta_3}{3} \right) \\ &+ C_F n_f T_F \left( -\frac{55}{3} + 16\zeta_3 \right) + n_f^2 T_F^2 \left( \frac{400}{81} - \frac{8\pi^2}{27} \right). \end{aligned} \quad (60)$$

Following the approach shown in Ref [19], the RG-improved jet function at an arbitrary scale  $\mu$  can be obtained

$$J_i(p^2, \mu) = \exp[-4C_i S(\mu_j, \mu) + 2a^{J_i}(\mu_j, \mu)] \tilde{j}(\partial_{\eta_j}, \mu_j) \frac{1}{p^2} \left( \frac{p^2}{\mu_j^2} \right)^{\eta_j} \frac{e^{-\gamma_E \eta_j}}{\Gamma(\eta_j)}, \quad (61)$$

where  $\eta_j = 2a_\Gamma(\mu_j, \mu)$ ,  $C_g = 3$ ,  $C_q = 4/3$ .

### C. Soft function

The soft function  $\mathcal{S}(k, \mu)$ , which describes soft interactions between all colored particles, can be calculated perturbatively in SCET. For the gg channel, the soft function is defined as

$$\langle 0 | \bar{\mathbf{T}}[Y_J^\dagger Y_2^\dagger Y_1^\dagger(x_-)] \mathbf{T}[Y_1 Y_2 Y_J(0)] | 0 \rangle = \int_0^\infty dk_+ e^{-ik_+(\bar{n}_J \cdot x)/2} S_{gg}(k_+) \quad (62)$$

For our threshold resummation at large  $p_T$ , the soft function becomes scaleless in dimensional regularization, which is consistent with the regularization scheme of hard function and jet function. Actually, we only need to calculate the emission diagrams, using dimensional regularization. The soft function  $\mathcal{S}(k, \mu)$ , similar to the jet function, satisfies the RG equation [19, 56]

$$\frac{d}{d \ln \mu} \mathcal{S}(k, \mu) = \left[ -4C_{gi} \gamma_{\text{cusp}} \ln \frac{k}{\tilde{\mu}} + 2\gamma^S \right] \mathcal{S}(k, \mu) + 4C_{gi} \gamma_{\text{cusp}} \int_0^k dk' \frac{\mathcal{S}(k, \mu) - \mathcal{S}(k', \mu)}{k - k'}. \quad (63)$$

According to the method shown in Refs. [19, 56], the RG-improved soft function can be given as

$$\mathcal{S}(k, \mu) = \exp[-4C_{gi} S(\mu_s, \mu) - 2a^S(\mu_s, \mu)] \tilde{s}(\partial_{\eta_s}, \mu_s) \frac{1}{k} \left( \frac{k}{\tilde{\mu}_s} \right)^{\eta_s} \frac{e^{-\gamma_E \eta_s}}{\Gamma(\eta_s)}, \quad (64)$$

where  $\eta_s = 2a_\Gamma(\mu_s, \mu)$ ,  $C_{gg} = 3/2$ ,  $C_{gq} = 3/2$ , and the Laplace transformed soft function  $\tilde{s}(L, \mu)$  at NNLO is given by [57]

$$\begin{aligned} \tilde{s}(L, \mu) = & 1 + \frac{\alpha_s}{4\pi} \left( 2C_{gi} \Gamma_0 L^2 - 2\gamma_0^S L + c_1^S \right) \\ & + \left( \frac{\alpha_s}{4\pi} \right)^2 \left\{ 2C_{gi}^2 \Gamma_0^2 L^4 + (-4\gamma_0^S C_{gi} \Gamma_0 - \frac{4\beta_0 C_{gi} \Gamma_0}{3}) L^3 \right. \\ & \left. + [2C_{gi} \Gamma_1 + 2(\gamma_0^S + \beta_0) \gamma_0^S + 2c_1^S C_{gi} \Gamma_0] L^2 - 2[\gamma_1^S + (\gamma_0^S + \beta_0) c_1^S] L + c_2^S \right\}. \end{aligned} \quad (65)$$

with

$$c_1^S = \pi^2 C_A / 2 \quad (66)$$

and

$$c_2^S = \left( \frac{1214}{81} + \frac{335\pi^2}{108} - \frac{11\zeta_3}{9} - \frac{41\pi^4}{120} \right) C_A^2 + \left( -\frac{328}{81} - \frac{25\pi^2}{27} + \frac{4\zeta_3}{9} \right) C_A n_f T_F. \quad (67)$$

### D. Scale independence

In the factorization formalism, we have introduced the hard function, jet function and soft function. Each of them is evaluated at a scale to make the perturbative expansion reliable, and then evolved to a common scale  $\mu_F$  in the PDFs. Therefore, it is important to check the scale independence of the final results. In fact, after expanding the exponent in Eq. (48), we can find the dependence on the intermediate scale  $\mu_h$  cancel each other up to  $\mathcal{O}(\alpha_s)$ . For the dependence of the jet scale, it is more complicate due to the appearance of the partial derivative operator and the delta function in the expansion of the jet function

$$\frac{1}{p^2} \left( \frac{p^2}{\mu_j^2} \right)^{\eta_j} = \frac{\delta(p^2)}{\eta_j} + \left[ \frac{1}{p^2} \right]_{\star}^{[p^2, \mu_j^2]} + \eta_j \left[ \frac{\ln(p^2/\mu_j^2)}{p^2} \right]_{\star}^{[p^2, \mu_j^2]} + \mathcal{O}(\eta_j^2). \quad (68)$$

The star distribution is defined as

$$\int_0^{Q^2} dp^2 \left[ \frac{1}{p^2} \left( \frac{p^2}{\mu^2} \right)^{\eta} \right]_{\star} f(p^2) = \int_0^{Q^2} dp^2 \frac{f(p^2) - f(0)}{p^2} \left( \frac{p^2}{\mu^2} \right)^{\eta} + \frac{f(0)}{\eta} \left( \frac{Q^2}{\mu^2} \right)^{\eta}, \quad (69)$$

where  $f(p^2)$  is a smooth test function, and the  $f(0)$  subtraction term is needed only if  $\eta < 0$ . The scale independence happens for the jet function only in the sense of the integration over  $p^2$ . For the dependence of the soft scale, it is the same as the jet function, and we do not discuss it here.

Now we begin to discuss the dependence of the the final results. Using the hadronic threshold definition in Eq. (10) and the cross section near the threshold in Eq. (30), we have

$$\frac{d\sigma}{dS_4 dy} \propto \int dx_a dx_b \int dp_1^2 \int dk^+ \frac{1}{\hat{s}} f_{i/P_a}(x_a, \mu) f_{j/P_b}(x_b, \mu) H_{ij}(\mu) J(p_1^2, \mu) S(k^+, \mu) \delta(S_4 - (-\hat{t})(1-x_a) - (-\hat{u})(1-x_b) - p_1^2 - 2k^+ E_1), \quad (70)$$

where we have changed the integration variables  $d\hat{t}d\hat{u}$  to  $dS_4 dy$ . From this equation, we can see clearly the connection between the threshold region of the whole system, represented by  $S_4$ , and those of the parts of the system, represented by  $(1-x_a), (1-x_b), p_1^2, k^+$  respectively. For simplifying the convolution form, using the Laplace transformation, the above equation can be written as

$$\frac{d\tilde{\sigma}}{dQ^2 dy} = \int_0^{\infty} dS_4 \exp\left(-\frac{S_4}{Q^2 e^{\gamma_E}}\right) \frac{d\sigma}{dS_4 dy}. \quad (71)$$

The Laplace transformed PDFs near the end point are given by

$$\tilde{f}_{i/P}(\tau, \mu) = \int_0^1 dx \exp\left(-\frac{1-x}{\tau e^{\gamma_E}}\right) f_{i/P_a}(x, \mu), \quad (72)$$

which satisfies RG equation

$$\frac{d}{d \ln \mu} \tilde{f}_{i/P}(\tau, \mu) = \left( 2C_{i\gamma_{\text{cusp}}} \ln(\tau) + 2\gamma^{\phi i} \right) \tilde{f}_{i/P}(\tau, \mu). \quad (73)$$

The variable  $\tau$  in the Laplace transformed PDF is given by

$$\tau_a = \frac{Q^2}{-\hat{t}} \quad \text{for} \quad \tilde{f}_{i/P_a}(\tau_a, \mu), \quad \text{and} \quad \tau_b = \frac{Q^2}{-\hat{u}} \quad \text{for} \quad \tilde{f}_{j/P_b}(\tau_b, \mu). \quad (74)$$

Using the relations between the anomalous dimensions presented in Ref. [47], we have

$$\frac{d}{d \ln \mu} \left[ \tilde{f}_{g/P_a}(\tau_a, \mu) \tilde{f}_{g/P_b}(\tau_b, \mu) \hat{\sigma}_{gg,B}(\mu) H_{gg}(\mu) \tilde{j}_g(\ln \frac{Q^2}{\mu^2}, \mu) \tilde{s}(\ln \frac{Q^2 \sqrt{\hat{s}}}{\mu \sqrt{\hat{t}\hat{u}}}, \mu) \right] = 0 \quad (75)$$

and

$$\frac{d}{d \ln \mu} \left[ \tilde{f}_{g/P_a}(\tau_a, \mu) \tilde{f}_{q/P_b}(\tau_b, \mu) \hat{\sigma}_{gq,B}(\mu) H_{gq}(\mu) \tilde{j}_q(\ln \frac{Q^2}{\mu^2}, \mu) \tilde{s}(\ln \frac{Q^2 \sqrt{\hat{s}}}{\mu \sqrt{\hat{t}\hat{u}}}, \mu) \right] = 0, \quad (76)$$

which show the scale independence of the cross section.

### E. Final RG-improved differential cross section

Combining the RG-improved hard, soft and jet functions, and using the identities [58]

$$\begin{aligned} a_\Gamma(\mu_1, \mu_2) + a_\Gamma(\mu_2, \mu_3) &= a_\Gamma(\mu_1, \mu_3), \\ S(\mu_1, \mu_2) + S(\mu_2, \mu_3) &= S(\mu_1, \mu_3) + \ln \frac{\mu_1}{\mu_2} a_\Gamma(\mu_2, \mu_3), \\ f(\partial_\eta) X^\eta &= X^\eta f(\ln X + \partial_\eta), \end{aligned} \quad (77)$$

we get the resummed differential cross section for the Higgs boson and a jet associated production

$$\begin{aligned} \frac{d\hat{\sigma}_{ij}^{\text{thres}}}{d\hat{t}d\hat{u}} &= \sum_{ij} \frac{\lambda_{0,ij}(\mu_h)}{16\pi\hat{s}^2} \\ &\exp[4\rho_{ij}S(\mu_h, \mu) - 2a_{ij}^V(\mu_h, \mu)] \tilde{H}_{ij}(\mu_h) \\ &\exp[-4C_i S(\mu_j, \mu) + 2a^{J_i}(\mu_j, \mu)] \left( \frac{M_H^2}{\mu_j^2} \right)^{\eta_j} \\ &\exp[-4C_{gi} S(\mu_s, \mu) - 2a^S(\mu_s, \mu)] \left( \frac{M_H^2 \sqrt{\hat{s}}}{\mu_s \sqrt{\hat{t}\hat{u}}} \right)^{\eta_s} \\ &\tilde{j}(\partial_\eta + L_j, \mu_j) \tilde{s}(\partial_\eta + L_s, \mu_s) \frac{1}{s_4} \left( \frac{s_4}{M_H^2} \right)^\eta \frac{e^{-\gamma_E \eta}}{\Gamma(\eta)}, \end{aligned} \quad (78)$$

where  $C_g = 3, C_q = 4/3, C_{gg} = 3/2, C_{gq} = 3/2, \eta = \eta_j + \eta_s, L_j = \ln(M_H^2/\mu_j^2)$  and  $L_s = \ln(M_H^2 \sqrt{\hat{s}})/(\mu_s \sqrt{\hat{t}\hat{u}})$ .

In order to compare with the fixed-order results, setting  $\mu_h = \mu_j = \mu_s = \mu$ , we expand the above results up to  $\mathcal{O}(\alpha_s^2)$

$$\begin{aligned} \left( \frac{\lambda_{0,ij}}{16\pi\hat{s}^2} \right)^{-1} \frac{d\hat{\sigma}_{ij}^{\text{thres}}}{d\hat{t}d\hat{u}} &= \delta(s_4) + \frac{\alpha_s}{4\pi} \left\{ A_2 D_2 + A_1 D_1 + A_0 \delta(s_4) \right\} \\ &+ \left( \frac{\alpha_s}{4\pi} \right)^2 \left\{ B_4 D_4 + B_3 D_3 + B_2 D_2 + B_1 D_1 + B_0 \delta(s_4) \right\}, \end{aligned} \quad (79)$$



with

$$D_n = \left[ \frac{\ln^{n-1}(s_4/M_H^2)}{s_4} \right]_+, \quad (80)$$

where the coefficients of  $A_n$  and  $B_n$  are given by

$$A_2 = (C_i + 4C_{gi})\Gamma_0, \quad (81)$$

$$A_1 = (C_i L_j + 4C_{gi} L_s)\Gamma_0 + \gamma_0^{J_i} - 2\gamma_0^S, \quad (82)$$

$$A_0 = \left[ \frac{1}{2}C_i L_j^2 + 2C_{gi} L_s^2 - \frac{\pi^2}{12}(C_i + 4C_{gi}) - \frac{\rho_{ij}}{2}L_H^2 \right] \Gamma_0 + \gamma_0^{J_i} L_j - 2\gamma_0^S L_s \\ + \tilde{\gamma}_0^{H_{ij}} L_H + c_1^{J_i} + c_1^S + c_1^H, \quad (83)$$

$$B_4 = \frac{A_2^2}{2}, \quad (84)$$

$$B_3 = \frac{3}{2}A_2 A_1 - \frac{1}{2}\beta_0(C_i + 8C_{gi})\Gamma_0, \quad (85)$$

$$B_2 = A_1^2 + A_2 \left( A_0 - \frac{\pi^2}{6}A_2 \right) - \beta_0[(C_i L_j + 8C_{gi} L_s)\Gamma_0 + \gamma_0^{J_i} - 4\gamma_0^S] + (C_i + 4C_{gi})\Gamma_1, \quad (86)$$

$$B_1 = \zeta_3 A_2^2 + A_1 \left( A_0 - \frac{\pi^2}{6}A_2 \right) \\ - \beta_0 \left[ \frac{\Gamma_0}{2}(C_i L_j^2 + 8C_{gi} L_s^2) - \frac{\pi^2 \Gamma_0}{12}(C_i + 8C_{gi}) + \gamma_0^{J_i} L_j - 4\gamma_0^S L_s + c_1^{J_i} + 2c_1^S \right] \\ + (C_i L_j + 4C_{gi} L_s)\Gamma_1 + \gamma_1^{J_i} - 2\gamma_1^S, \quad (87)$$

$$B_0 = \frac{A_0^2}{2} - \frac{\pi^4}{720}A_2^2 - \frac{\Gamma_0^2}{12}(C_i L_j + 4C_{gi} L_s)[\pi^2(C_i L_j + 4C_{gi} L_s) - 12\zeta_3(C_i + 4C_{gi})] \\ - \frac{\Gamma_0}{6}(\gamma_0^{J_i} - 2\gamma_0^S)[\pi^2(C_i L_j + 4C_{gi} L_s) - 6\zeta_3(C_i + 4C_{gi})] + \rho_{ij}\tilde{\gamma}_0^{H_{ij}}\Gamma_0 L_H^3 \\ - \frac{\pi^2}{12}[\Gamma_1(C_i + 4C_{gi}) + (\gamma_0^{J_i} - 2\gamma_0^S)^2] + \frac{\Gamma_1}{2}(C_i L_j^2 + 4C_{gi} L_s^2 - \rho_{ij}L_H^2) \\ + (\gamma_1^{J_i} L_j - 2\gamma_1^S L_s - L_H \tilde{\gamma}_1^{H_{ij}} - 2c_1^H \tilde{\gamma}_0^{H_{ij}} L_H) - \frac{1}{2}(c_1^{J_i^2} + c_1^{S^2} + c_1^{H^2}) + c_2^{J_i} + c_2^S + c_2^H \\ + \frac{\beta_0}{12}\{\Gamma_0[C_i(-2L_j^3 + \pi^2 L_j - 4\zeta_3) + 8C_{gi}(-2L_s^3 + \pi^2 L_s - 4\zeta_3) - 2\rho_{ij}L_H^3] \\ + \pi^2(\gamma_0^{J_i} - 4\gamma_0^S) - 6(\gamma_0^{J_i} L_j^2 - 4\gamma_0^S L_s^2 + 2c_1^J L_j + 4c_1^S L_s) - 12c_1^H L_H + 6\tilde{\gamma}_0^{H_{ij}} L_H^2\}, \quad (88)$$

with  $\zeta_3 = 1.20206 \dots$ . We find that the coefficient  $A_{2,1,0}$  agree with the NLO results in Ref. [21].

In order to obtain the best possible precise predictions, we combine our resummed result with the nonsingular terms up to NLO in fixed-order perturbative calculations, and the RG-improved differential cross section are given by

$$\frac{d\hat{\sigma}_{\text{Resum}}}{d\hat{t}d\hat{u}} = \frac{d\hat{\sigma}^{\text{thres}}}{d\hat{t}d\hat{u}} + \left( \frac{d\hat{\sigma}_{\text{NLO}}}{d\hat{t}d\hat{u}} - \frac{d\hat{\sigma}^{\text{thres}}}{d\hat{t}d\hat{u}} \right) \Big|_{\text{expanded to NLO}}, \quad (89)$$

where the NLO results can be obtained by the modified Monte Carlo programs MCFM [59] or HNNLO [30, 60, 61]. Near the threshold regions, the expansion of the resummed results approaches

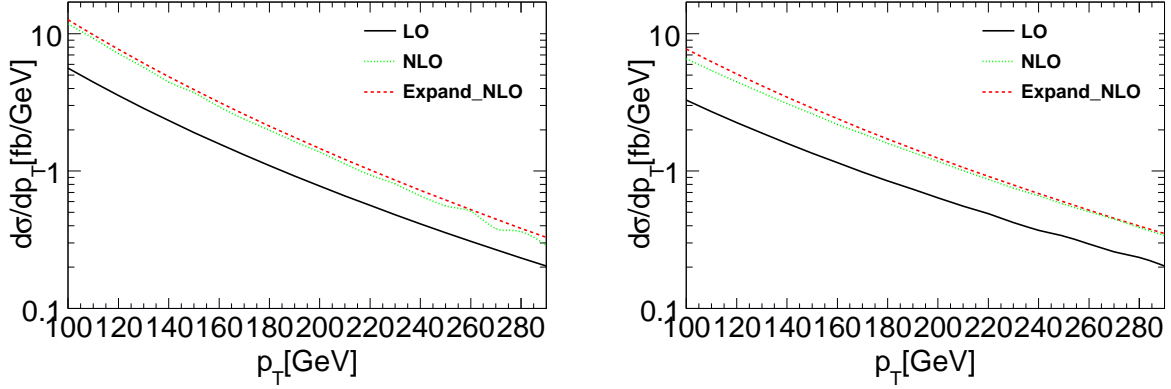


FIG. 3: The singular terms and fixed-order contribution of the  $gg$  channel(left) and  $gq$  channel (right) for the Higgs boson and a jet associated production with large  $p_T$  at the 8 TeV LHC.

the fixed-order one so that the terms in the bracket almost vanishes and the threshold contribution dominates. In the regions far from the threshold limit, the fixed-order contribution dominates and the resummation effects are not important.

## V. NUMERICAL DISCUSSION

In this section, we discuss the relevant numerical results. The Higgs boson mass and top quark mass are chosen as 125.6 and 173.2 GeV [62], respectively. The CTEQ6M PDF sets are used throughout our numerical calculations. And the factorization scale is set at  $M_H$  unless special statement. There are three new scales, i.e.,  $\mu_h, \mu_j, \mu_s$ , introduced in the SCET formalism. They should be properly chosen so that the corresponding hard functions, jet function and soft function have stable numerical results, which means each function should not contain large logarithms at the chosen scale.

Before discussing how to choose the different scales for obtaining the numerical RG-improved cross sections, it is necessary to examine to what extent the singular terms approximate the fixed-order calculations. In Fig. 3, we compare the contribution of the singular terms by expanding the resummation formalism with the LO and NLO results at the 8 TeV LHC. First, we find that the high order corrections for both the  $gg$  and  $gq$  channel Higgs boson production<sup>1</sup> are very large, which means that higher QCD corrections are important and needed to be included to give a reliable perturbative prediction. Second, we see that the NLO cross section is well approximated

<sup>1</sup> For simplicity, we have denoted the two subprocess of  $gq \rightarrow H + j$  and  $g\bar{q} \rightarrow H + j$  as  $gq$  channel.

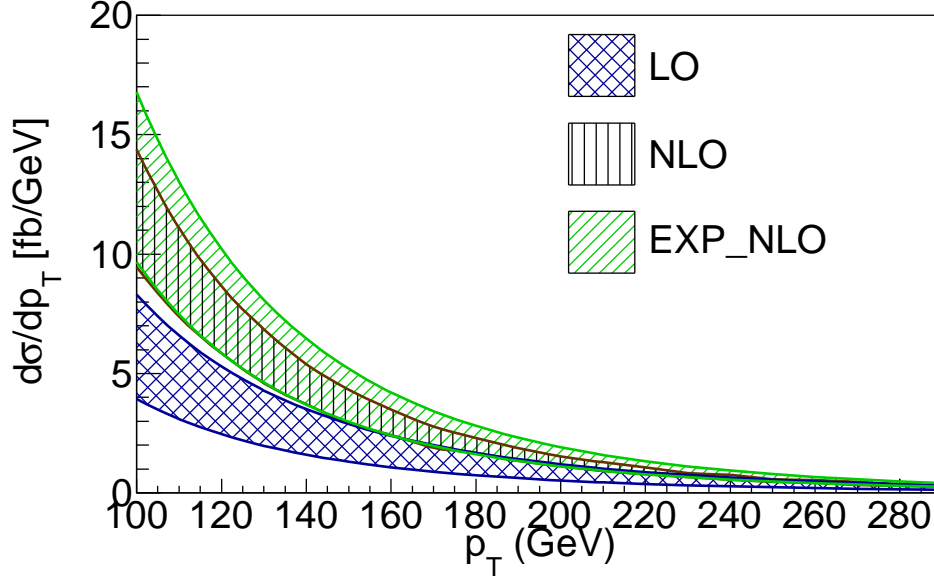


FIG. 4: The scale uncertainties of the LO, NLO, expanded NLO results varying the scale from  $M_H/2$  to  $2M_H$  for  $gg$  channel at the 8 TeV LHC.

by the singular terms when the  $p_T$  of the Higgs boson is larger than 100 (200) GeV for the  $gg$  ( $gq$ ) channel. Since one can not distinguish the quark jet (in  $gq$  channel) from the gluon jet (in  $gg$  channel), the two channels should be combined in order to compare with the experimental measurement. And because the  $gg$  channel dominates in the total and differential cross sections, we will present the resummed prediction for the Higgs boson production in the range  $p_T > 100$  GeV. These observations are also true after considering the scale uncertainties by varying the scale from  $M_H/2$  to  $2M_H$ , as shown in Fig. 4.

#### A. Scale choice and matching

In the above discussions, the cross section has been factorized into the hard function, jet function and soft function, and each function only depends on a single scale. So the hard scale, jet scale and soft scale can be chosen, respectively, at their intrinsic scales. Then using the RG, all scales evolve to the same factorization scale. In Fig. 5, we show the contribution to the NLO correction from only the hard function, normalized by the LO result, as a function of the hard scale. The hard function takes maximum values when the hard scale is around  $\sqrt{p_T^2 + M_H^2}$  for  $p_T = 100 \sim 250$  GeV. And the contributions from the hard function are very large, generally larger than 0.5 for  $p_T = 100 \sim 250$  GeV. This means that the hard function is very important, and needs to be calculated with higher precision. Resummation is a way to achieve this target. On the other hand,

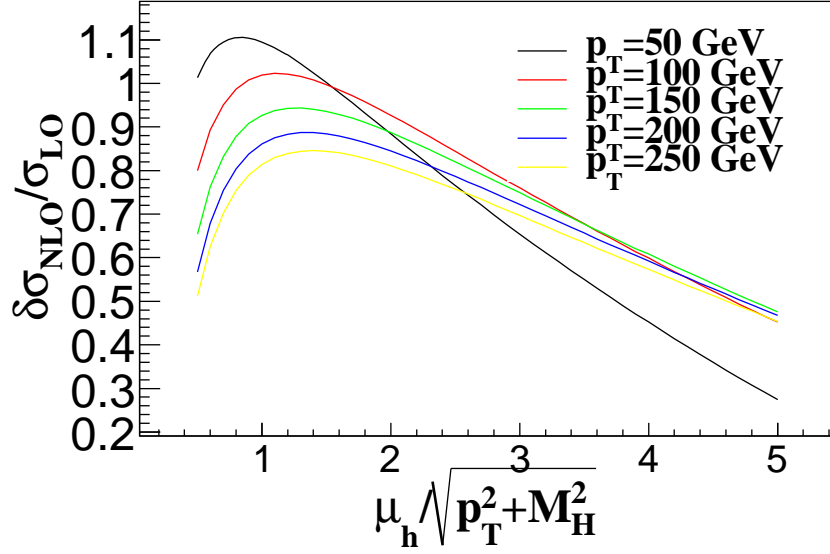


FIG. 5: The NLO contribution of the hard function for different  $p_T$  cuts at the 8 TeV LHC.

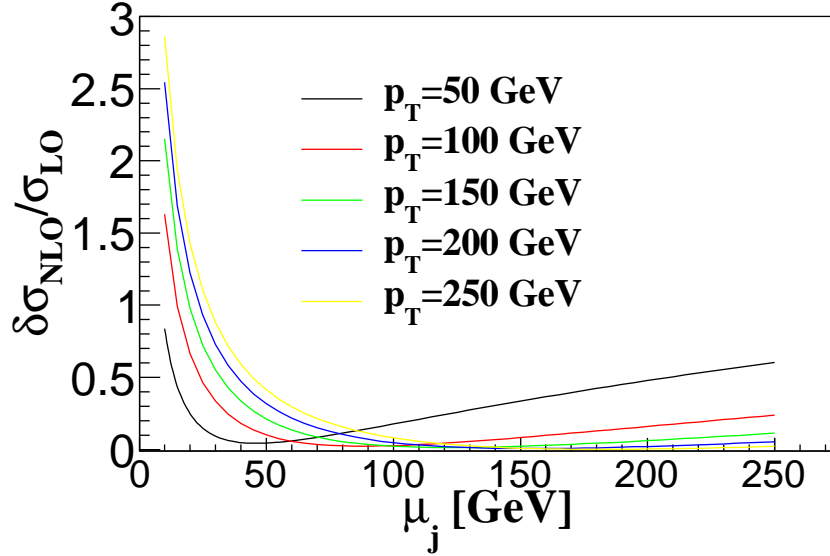


FIG. 6: The NLO contribution of the jet function for different  $p_T$  cuts at the 8 TeV LHC.

we also notice that the terms which can be resummed are only a limited part of the hard function. There is also significant contribution from those terms which are scale independent. Here, we choose  $2.5\sqrt{p_T^2 + M_H^2}$  as the default hard scale. The scale uncertainty of final resummed result from variation of the hard scale is about 12%, as shown in Fig. 8.

In Fig. 6, we show the contribution to the NLO correction from only the jet function, normalized

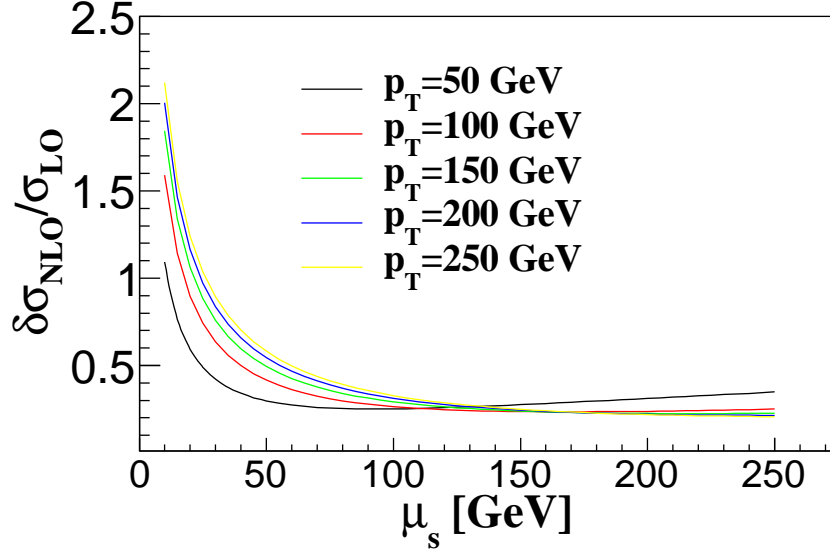


FIG. 7: The NLO contribution of the soft function for different  $p_T$  cuts at the 8 TeV LHC.

by the LO result, as a function of the jet scale. The jet function drops very quickly when the jet scale is smaller than 50 GeV, and changes very slowly when the jet scale is larger than 50 GeV. We can also see that the contribution from the jet function is about 10% if  $p_T$  is larger than 100 GeV. The soft function has a similar behavior, as shown in Fig. 7, except that the contribution from the soft function is about 30% if  $p_T$  is larger than 100 GeV. We choose  $\mu_j \approx 150$  GeV,  $\mu_s \approx 100$  GeV as the default jet and soft scales, respectively. The uncertainties of the final resummed result from the variation of jet and soft scales are about 2.4% and 5.8% as shown in Fig. 9 and Fig. 10, respectively.

Finally, to examine the factorization scale uncertainty in the final resummed result, we vary the factorization scale from  $M_H/2$  to  $2M_H$  and show the resummed result in Fig. 11. For comparison, we present scale uncertainties of the NLO result obtained by varying  $\mu = \mu_R = \mu_f = M_H$  by a factor of 2, as done in Ref. [29]. After matching the resummed result with the NLO one, as shown in Eq. 89, the result is shown in Fig. 12. We see that both the resummed and matched results have smaller scale uncertainties than the NLO result.

The case of  $gq$  channel is similar to the  $gg$  channel, and the scale uncertainty after resummation reduces more significantly compared with the  $gg$  channel; see Figs. 13,14. For the  $q\bar{q}$  channel, the contribution is very small. So we do not show its result individually.

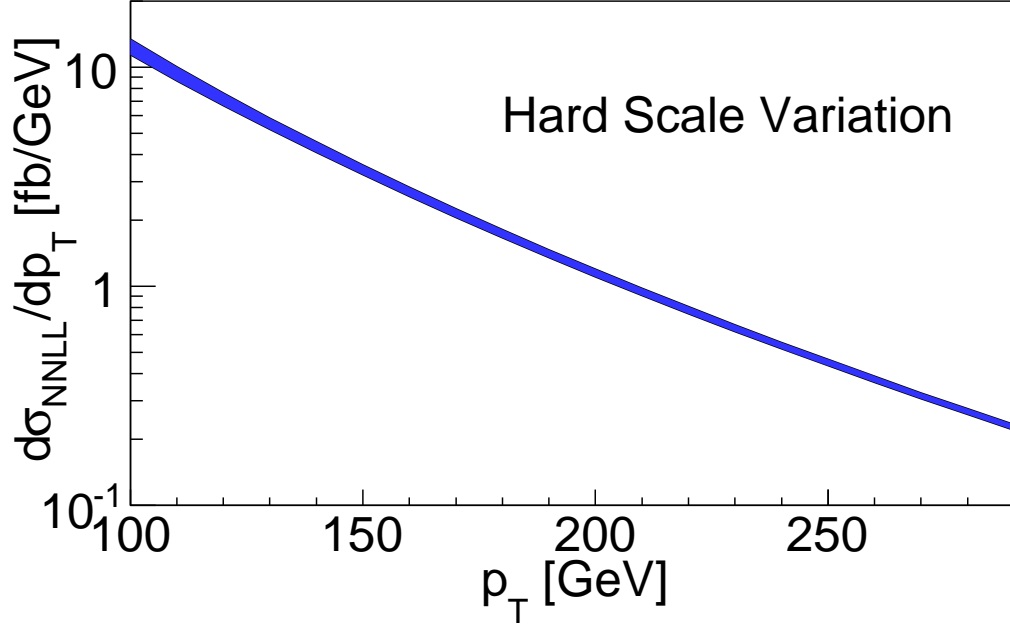


FIG. 8: The hard scale uncertainty of the resummation results at the 8 TeV LHC.

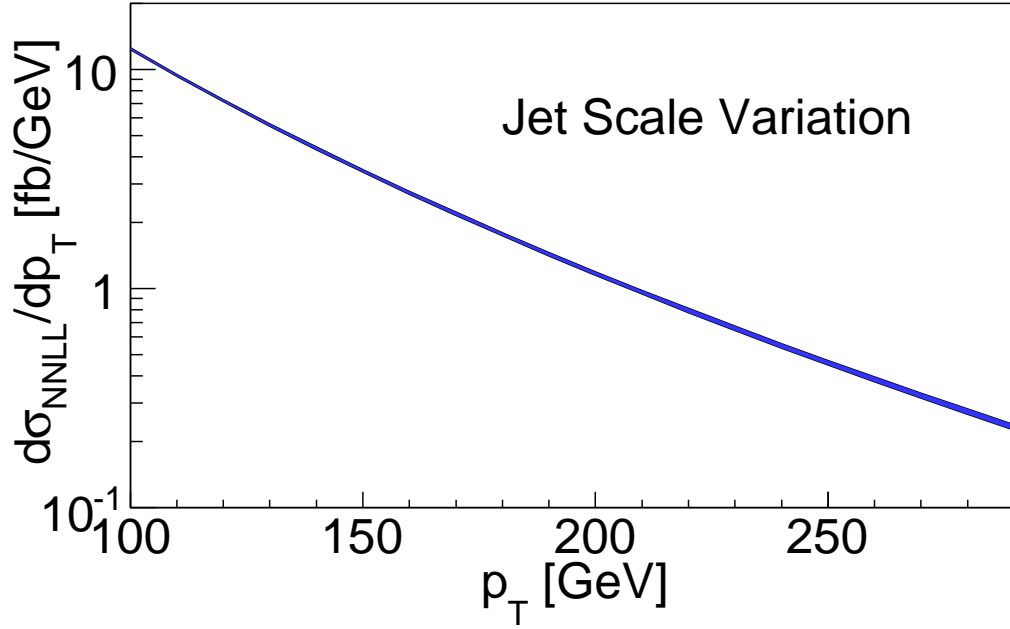


FIG. 9: The jet scale uncertainty of the resummation results at the 8 TeV LHC.

Figure 15 shows the differential cross section as a function of  $p_T$  after matching to the NLO results. The result with resummation effects obviously reduces the large scale uncertainty compared to the NLO result. The ratio of the resummation result to the LO cross section is sensitive to  $p_T$ ,

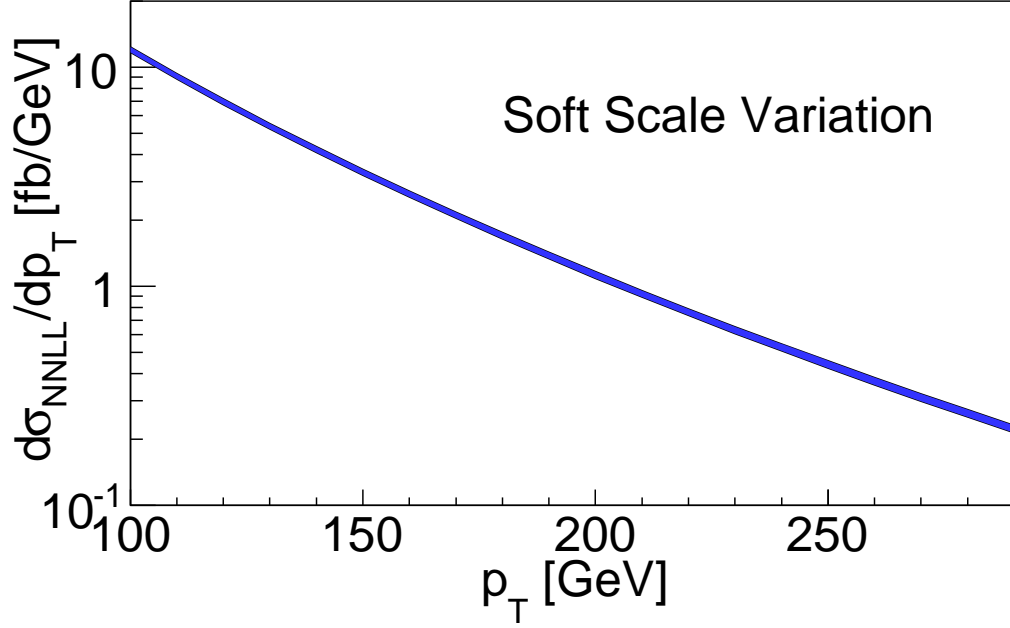


FIG. 10: The soft scale uncertainty of the resummation results at the 8 TeV LHC.

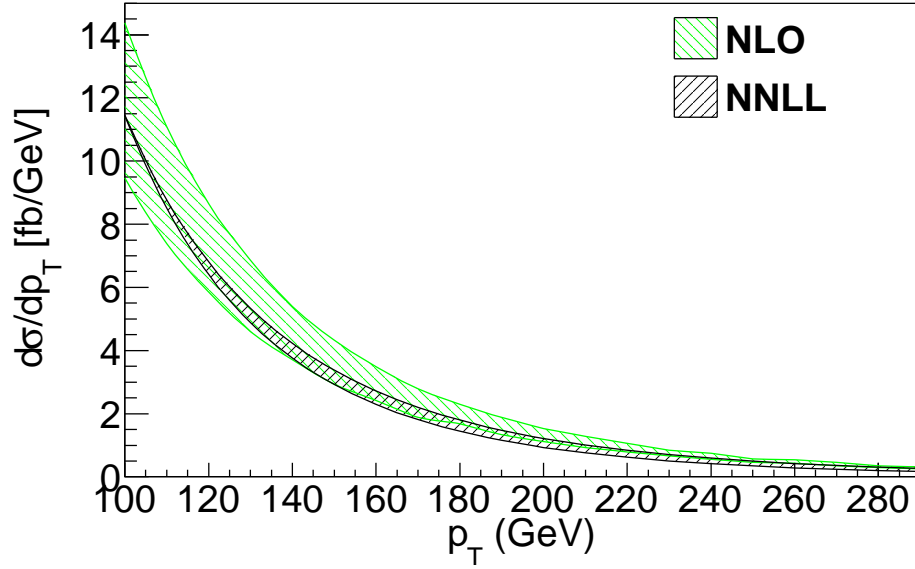


FIG. 11: The scale uncertainty of the NNLL and NLO results for the Higgs boson and one jet associated production with large  $p_T$  at the 8 TeV LHC for gg channel.

changing from 1.8 to 1.0 as  $p_T$  varies from 100 to 290 GeV. The resummation results of the total cross section decrease the NLO one by about 11% at the default scales when the Higgs boson  $p_T$  is larger than 100 GeV.

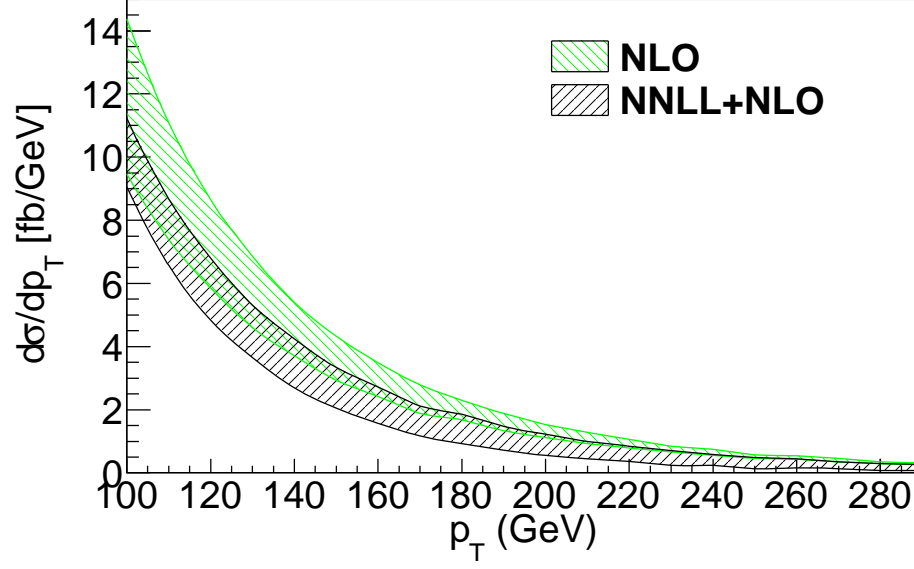


FIG. 12: The scale uncertainty of the matched and NLO results for the Higgs boson and one jet associated production with large  $p_T$  at the 8 TeV LHC for the gg channel.

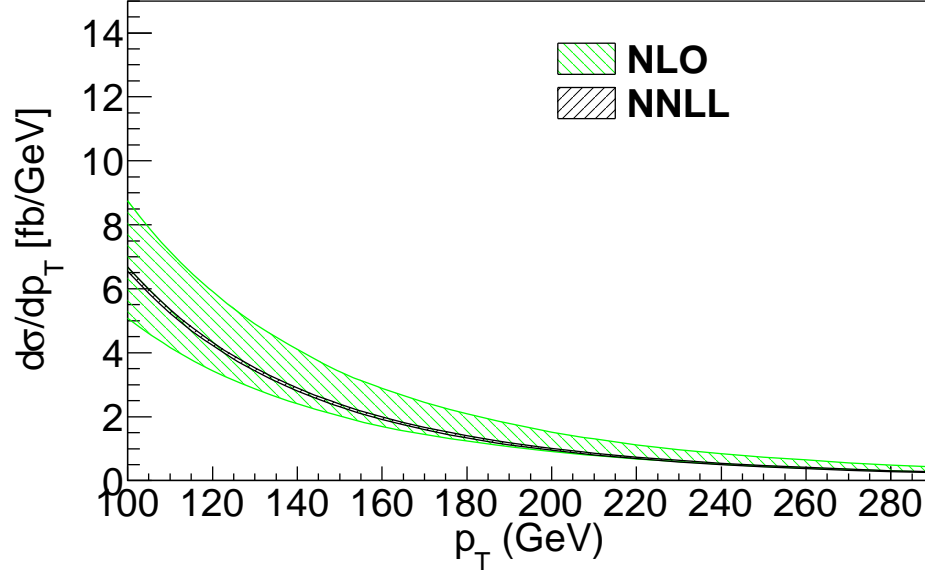


FIG. 13: The scale uncertainty of the NNLL and NLO results for the Higgs boson and one jet associated production with large  $p_T$  at the 8 TeV LHC for gq channel.

### B. Discussion on the finite top quark mass effects

Up to now, the discussion is under the assumption of infinite top quark mass limit. However, in the case of large  $p_T$  Higgs boson production, the Higgs low energy theorem [63, 64] may fail to apply, and the top quark mass effects may make a sense. Considering the finite top quark mass will



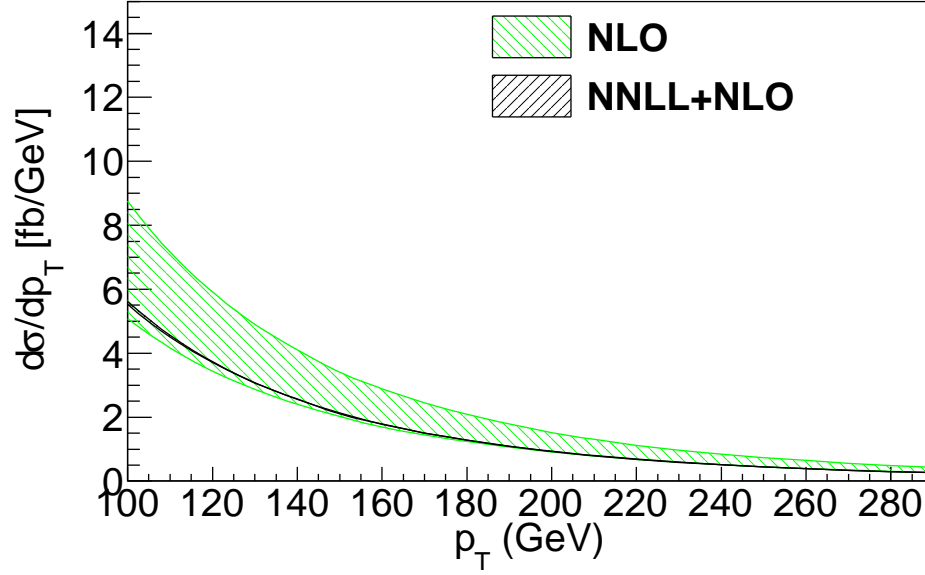


FIG. 14: The scale uncertainty of the matched and NLO results for the Higgs boson and one jet associated production with large  $p_T$  at the 8 TeV LHC for the gq channel.

bring more complicated calculations, but also open a new way to probe the coupling of the Higgs to top quarks. When including the finite top quark mass, there exists only LO results [23, 24] and the corresponding parton shower effects [32, 65]. Unfortunately, there is no complete QCD NLO calculations of the Higgs plus jet including exact top mass effects. Only the subleading terms in  $1/m_t$  have been calculated at QCD NLO [22, 30]. It is found that the infinite top quark mass limit is a very good approximation as long as  $p_T < 200$  GeV [21, 22]. Other discussions can be seen in Refs. [22, 66, 67]. We investigate the possible top quark mass effects by using the program HNNLO, presenting the results in Figs.16. For Higgs's  $p_T$  less than 200 GeV, the finite top quark mass effects are not obvious (the difference between the results with and without finite top quark mass is less than 4%). For the  $p_T$  larger than 200 GeV, the top quark mass begins to make sense and it is necessary to consider the finite top quark mass effects. We define the differential  $K$  factor as

$$K(p_T) = \frac{d\sigma_{\infty}^{NLO+NNLL}}{d\sigma_{\infty}^{LO}}, \quad (90)$$

where  $\infty$  refers to the infinite top quark mass limit. Since the differential  $K$  factor depends weakly on the top quark mass [25, 68, 69], we can obtain a reliable approximation of higher-order cross section by multiplying the  $K$  factor to the exact top mass dependent LO one following the methods

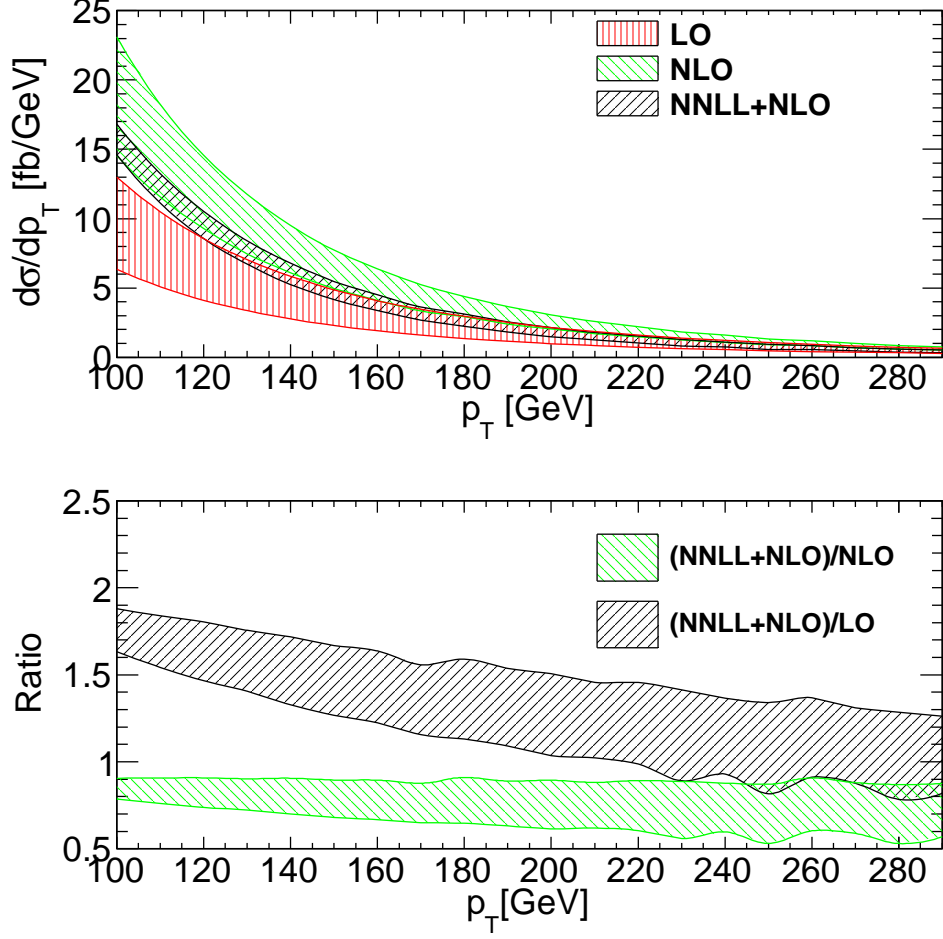


FIG. 15: The total scale uncertainty of the matched and NLO results for the single Higgs production with large  $p_T$  at the 8 TeV LHC.

in Refs. [30, 70], which is given by

$$\frac{d\sigma}{dp_T} = \frac{d\sigma_{m_t}^{LO}}{dp_T} K(p_T). \quad (91)$$

Here,  $\sigma_{m_t}^{LO}$  means the exact LO cross section with finite top quark mass. The obtained  $p_T$  distribution of the Higgs boson at NNLL+NLO with finite top quark mass is shown in Fig. 16 as the black curve at the central value of the scales. In Fig. 16, we compare the resummation results with NLO ones in both cases of infinite and finite top quark mass. These results can be used to improve the accuracy in probing the Higgs couplings to top quarks in the recent works [5–7].

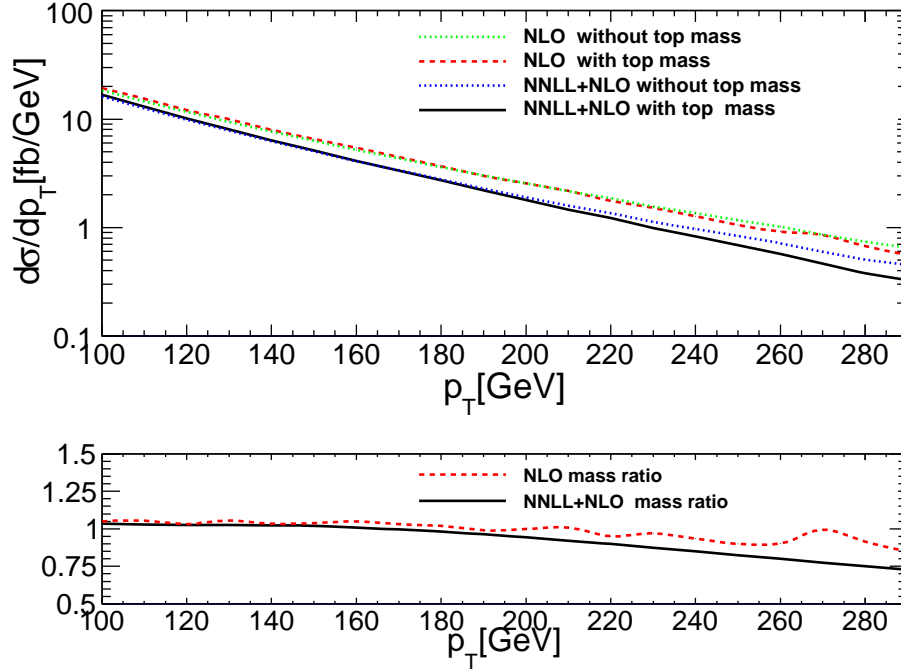


FIG. 16: The central value ( $\mu_F = M_H, \mu_h = 2.5\sqrt{p_T^2 + M_H^2}, \mu_j = 150$  GeV,  $\mu_s = 100$  GeV) of four cases for the large  $p_T$  Higgs boson production at the 8 TeV LHC. The green curve is the NLO  $p_T$  distribution in the infinite top quark mass limit, the red curve is the NLO one with top mass effects, the blue curve is the NNLL+NLO one in the infinite top quark mass limit and the black curve is the NNLL+NLO with top quark mass effects.

### C. Simple discussions on higher order corrections

After our paper appeared as an e-print, the authors in Ref. [71] investigated the same process and included the two-loop hard function. Their NNNLL results are not matched to the NNLO fixed order results in their paper. We use SCET to resum the large logarithm and match to the NLO fixed order one, while the authors in Ref. [71] use SCET to predict the approximated NNLO result, and their main conclusion is that the approximated NNLO correction increases the NLO by 50%. The expanded NNLO<sub>p</sub> results with the one-loop hard function squared (NNLO singular terms expanded from one-loop hard function, two-loop jet function, and two loop soft function) is shown in Fig. 17, and we see that the expanded NNLO<sub>p</sub> result with the one loop hard function squared increases the NLO one significantly. The reason is that the main contribution to the two-loop hard function is from the squared one-loop hard function, shown as  $A_0^2$  term in  $B_0$  from Eq.(88). Besides, our results of LO and NLO singular terms are exactly the same as their results if we choose the same parameters as in [71].

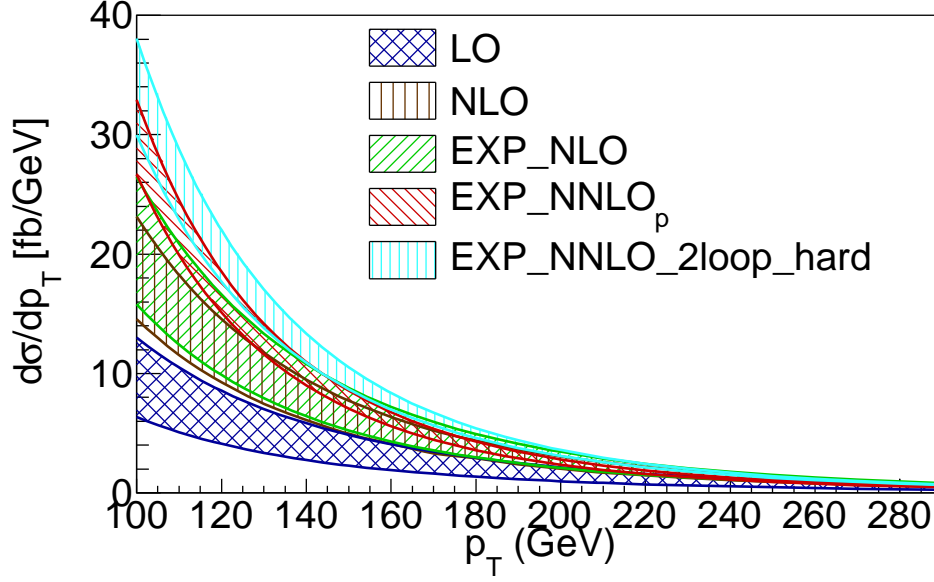


FIG. 17: The total scale uncertainties of the LO, NLO, expanded NLO, expanded NNLO<sub>p</sub> (with one-loop hard function squared), and expanded NNLO (with the two-loop hard function ) results varying the scale from  $M_H/2$  to  $2M_H$  with all channels at the 8 TeV LHC.

Furthermore, we incorporate the two-loop hard function extracted from Refs.[20, 53], and find that the expanded NNLO results with two-loop hard function (NNLO singular terms from two-loop hard function, two-loop jet function and two-loop soft function) are numerically identical to the ones in Ref. [71] when the same parameters are chosen. The expanded NNLO result with two-loop hard function is shown in Fig. 17, where the term  $c_2^H - c_1^{H^2}/2$  is added in order to compare with the expanded NNLO<sub>p</sub> result with one-loop hard function squared. Figure 17 shows that the difference between the two kinds of expanded NNLO results is not very large. This is because the dominant contribution comes from the large logarithm terms which are obtained by expansion of the RG evolution expression, not the  $c_2^H - c_1^{H^2}/2$ . At NNLL order with the default scales, the contribution of negative logarithm terms in  $A_0$  dominates, and this leads to the fact that the resummation effects decrease the NLO cross section. After expanding the cross section to NNLO order, new positive logarithms, such as  $A_0^2$  terms in  $B_0$ , overwhelm the negative ones. Thus, the corrections for the two kinds of expanded NNLO results with the one-loop and two-loop hard function, respectively, become positive as shown in Fig.17, whether the  $c_2^H - c_1^{H^2}/2$  term is included or not. The NNNLL resummation effect matched to NNLO fixed order deserves to be studied further, but is beyond the scope of this paper, and left for future work.

## VI. CONCLUSION

We have studied the Higgs boson production at large  $p_T$  at the LHC, including the resummation effects in SCET. We find that the resummation effects decrease the NLO cross sections by about 11% at the central values of the scales when the Higgs boson  $p_T$  is larger than 100 GeV, and also reduce the scale uncertainty obviously. Moreover, we discuss the top mass effects numerically, and find that the top quark mass effects increase with the increasing of  $p_T$ . The  $p_T$  distribution of Higgs boson is important for describing the Higgs boson production at the LHC, and it is sensitive to the QCD higher order corrections. A precise measurement of the Higgs  $p_T$  is expected to be given in the near future and its precise prediction is very important for the experimental analyses. Thus, it is necessary to precisely investigate the large  $p_T$  behavior of the Higgs boson, and any deviation of the Higgs boson's  $p_T$  distribution will give hints to the possible modification of the Higgs couplings to the top quark, which will shed light on the new physics.

## Acknowledgments

This work was partially supported by the National Natural Science Foundation of China, under Grants No. 11375013 and No. 11135003. Jian Wang was supported by the Cluster of Excellence *Precision Physics, Fundamental Interactions and Structure of Matter* (PRISMA-EXC 1098).

- 
- [1] S. Chatrchyan et al. (CMS Collaboration), Phys.Lett. **B716**, 30 (2012), 1207.7235.
  - [2] G. Aad et al. (ATLAS Collaboration), Phys.Lett. **B716**, 1 (2012), 1207.7214.
  - [3] S. Chatrchyan et al. (CMS Collaboration), JHEP **1305**, 145 (2013), 1303.0763.
  - [4] R. V. Harlander and T. Neumann, Phys.Rev. **D88**, 074015 (2013), 1308.2225.
  - [5] A. Azatov and A. Paul, JHEP **1401**, 014 (2014), 1309.5273.
  - [6] A. Banfi, A. Martin, and V. Sanz, JHEP **1408**, 053 (2014), 1308.4771.
  - [7] C. Grojean, E. Salvioni, M. Schlaffer, and A. Weiler, JHEP **1405**, 022 (2014), 1312.3317.
  - [8] Tech. Rep. ATLAS-CONF-2014-011, CERN, Geneva (2014).
  - [9] D. de Florian, G. Ferrera, M. Grazzini, and D. Tommasini, JHEP **1111**, 064 (2011), 1109.2109.
  - [10] D. de Florian, A. Kulesza, and W. Vogelsang, JHEP **0602**, 047 (2006), hep-ph/0511205.
  - [11] X. Liu and F. Petriello, Phys.Rev. **D87**, 014018 (2013), 1210.1906.
  - [12] X. Liu and F. Petriello, Phys.Rev. **D87**, 094027 (2013), 1303.4405.
  - [13] R. Boughezal, X. Liu, F. Petriello, F. J. Tackmann, and J. R. Walsh, Phys.Rev. **D89**, 074044 (2014), 1312.4535.

- [14] T. T. Jouttenus, I. W. Stewart, F. J. Tackmann, and W. J. Waalewijn, Phys.Rev. **D88**, 054031 (2013), 1302.0846.
- [15] C. W. Bauer, S. Fleming, and M. E. Luke, Phys. Rev. **D63**, 014006 (2000), hep-ph/0005275.
- [16] C. W. Bauer, S. Fleming, D. Pirjol, and I. W. Stewart, Phys. Rev. **D63**, 114020 (2001), hep-ph/0011336.
- [17] C. W. Bauer and I. W. Stewart, Phys. Lett. **B516**, 134 (2001), hep-ph/0107001.
- [18] C. W. Bauer, D. Pirjol, and I. W. Stewart, Phys. Rev. **D65**, 054022 (2002), hep-ph/0109045.
- [19] T. Becher and M. Neubert, Phys. Rev. Lett. **97**, 082001 (2006), hep-ph/0605050.
- [20] T. Becher, G. Bell, C. Lorentzen, and S. Marti, JHEP **1402**, 004 (2014), 1309.3245.
- [21] V. Ravindran, J. Smith, and W. Van Neerven, Nucl.Phys. **B634**, 247 (2002), hep-ph/0201114.
- [22] R. V. Harlander, T. Neumann, K. J. Ozeren, and M. Wiesemann, JHEP **1208**, 139 (2012), 1206.0157.
- [23] R. K. Ellis, I. Hinchliffe, M. Soldate, and J. van der Bij, Nucl.Phys. **B297**, 221 (1988).
- [24] U. Baur and E. N. Glover, Nucl.Phys. **B339**, 38 (1990).
- [25] R. V. Harlander and K. J. Ozeren, JHEP **0911**, 088 (2009), 0909.3420.
- [26] C. R. Schmidt, Phys.Lett. **B413**, 391 (1997), hep-ph/9707448.
- [27] D. de Florian, M. Grazzini, and Z. Kunszt, Phys.Rev.Lett. **82**, 5209 (1999), hep-ph/9902483.
- [28] C. J. Glosser and C. R. Schmidt, JHEP **0212**, 016 (2002), hep-ph/0209248.
- [29] R. Boughezal, F. Caola, K. Melnikov, F. Petriello, and M. Schulze, JHEP **1306**, 072 (2013), 1302.6216.
- [30] M. Grazzini and H. Sargsyan, JHEP **1309**, 129 (2013), 1306.4581.
- [31] U. Langenegger, M. Spira, A. Starodumov, and P. Trueb, JHEP **0606**, 035 (2006), hep-ph/0604156.
- [32] E. Bagnaschi, G. Degrossi, P. Slavich, and A. Vicini, JHEP **1202**, 088 (2012), 1111.2854.
- [33] C. Arnesen, I. Z. Rothstein, and J. Zupan, Phys.Rev.Lett. **103**, 151801 (2009), 0809.1429.
- [34] E. Laenen, G. Oderda, and G. Sterman, Phys. Lett. **B438**, 173 (1998), hep-ph/9806467.
- [35] M. Beneke, P. Falgari, and C. Schwinn, Nucl. Phys. **B828**, 69 (2010), 0907.1443.
- [36] T. Becher and M. D. Schwartz, JHEP **02**, 040 (2010), 0911.0681.
- [37] J. C. Collins, D. E. Soper, and G. F. Sterman, Nucl.Phys. **B250**, 199 (1985).
- [38] J. Collins, Cambridge monographs on particle physics, nuclear physics and cosmology.32 (2011).
- [39] P. Sun, C. P. Yuan, and F. Yuan (2014), 1409.4121.
- [40] A. V. Manohar, Phys. Rev. **D68**, 114019 (2003), hep-ph/0309176.
- [41] A. Idilbi and X.-d. Ji, Phys.Rev. **D72**, 054016 (2005), hep-ph/0501006.
- [42] V. Ahrens, A. Ferroglia, M. Neubert, B. D. Pecjak, and L. L. Yang, JHEP **1009**, 097 (2010), 1003.5827.
- [43] T. Becher and M. Neubert, Phys. Rev. **D79**, 125004 (2009), 0904.1021.
- [44] A. Ferroglia, M. Neubert, B. D. Pecjak, and L. L. Yang, Phys.Rev.Lett. **103**, 201601 (2009), 0907.4791.
- [45] A. Ferroglia, M. Neubert, B. D. Pecjak, and L. L. Yang, JHEP **0911**, 062 (2009), 0908.3676.
- [46] T. Becher and M. Neubert, Phys.Rev.Lett. **102**, 162001 (2009), 0901.0722.
- [47] T. Becher and M. Neubert, JHEP **0906**, 081 (2009), 0903.1126.
- [48] V. Ahrens, M. Neubert, and L. Vernazza, JHEP **1209**, 138 (2012), 1208.4847.
- [49] G. Korchemsky and A. Radyushkin, Nucl.Phys. **B283**, 342 (1987).

- [50] G. Korchemsky, Phys.Lett. **B220**, 629 (1989).
- [51] I. Korchemskaya and G. Korchemsky, Physics Letters B **287**, 169 (1992).
- [52] T. Becher, M. Neubert, and B. D. Pecjak, JHEP **01**, 076 (2007), hep-ph/0607228.
- [53] T. Gehrmann, M. Jaquier, E. Glover, and A. Koukoutsakis, JHEP **1202**, 056 (2012), 1112.3554.
- [54] T. Becher and M. Neubert, Phys. Lett. **B637**, 251 (2006), hep-ph/0603140.
- [55] T. Becher and G. Bell, Phys.Lett. **B695**, 252 (2011), 1008.1936.
- [56] T. Becher, M. Neubert, and G. Xu, JHEP **07**, 030 (2008), 0710.0680.
- [57] T. Becher, G. Bell, and S. Marti, JHEP **1204**, 034 (2012), 1201.5572.
- [58] T. Becher and M. D. Schwartz, JHEP **0807**, 034 (2008), 0803.0342.
- [59] J. M. Campbell and R. Ellis, Nucl.Phys.Proc.Suppl. **205-206**, 10 (2010), 1007.3492.
- [60] S. Catani and M. Grazzini, Phys.Rev.Lett. **98**, 222002 (2007), hep-ph/0703012.
- [61] M. Grazzini, JHEP **0802**, 043 (2008), 0801.3232.
- [62] M. Muether and CDF (Tevatron Electroweak Working Group, CDF Collaboration, D0 Collaboration) (2013), 1305.3929.
- [63] J. R. Ellis, M. K. Gaillard, and D. V. Nanopoulos, Nucl.Phys. **B106**, 292 (1976).
- [64] M. A. Shifman, A. Vainshtein, M. Voloshin, and V. I. Zakharov, Sov.J.Nucl.Phys. **30**, 711 (1979).
- [65] J. Alwall, Q. Li, and F. Maltoni, Phys.Rev. **D85**, 014031 (2012), 1110.1728.
- [66] S. Dittmaier, S. Dittmaier, C. Mariotti, G. Passarino, R. Tanaka, et al. (2012), 1201.3084.
- [67] I. W. Stewart, F. J. Tackmann, J. R. Walsh and S. Zuberi, Phys. Rev. D **89**, 054001 (2014), 1307.1808.
- [68] M. Spira, A. Djouadi, D. Graudenz, and P. Zerwas, Nucl.Phys. **B453**, 17 (1995), hep-ph/9504378.
- [69] A. Pak, M. Rogal, and M. Steinhauser, JHEP **1002**, 025 (2010), 0911.4662.
- [70] J. Grigo, J. Hoff, K. Melnikov and M. Steinhauser, PoS RADCOR **2013**, 006 (2013), 1311.7425.
- [71] T. Becher, G. Bell, C. Lorentzen and S. Marti, JHEP **1411**, 026 (2014), 1407.4111.